

1           **MOCHI enables discovery of heterogeneous interactome**  
2           **modules in 3D nucleome**

3           Dechao Tian<sup>1,#</sup>, Ruochi Zhang<sup>1,#</sup>, Yang Zhang<sup>1</sup>, Xiaopeng Zhu<sup>1</sup>, and Jian Ma<sup>1,\*</sup>

4           <sup>1</sup>Computational Biology Department, School of Computer Science,  
5           Carnegie Mellon University, Pittsburgh, PA 15213, USA

6           <sup>#</sup>These two authors contributed equally

7           <sup>\*</sup>Correspondence: [jianma@cs.cmu.edu](mailto:jianma@cs.cmu.edu)

8           **Contact**

9           To whom correspondence should be addressed:

10          Jian Ma  
11          School of Computer Science  
12          Carnegie Mellon University  
13          7705 Gates-Hillman Complex  
14          5000 Forbes Avenue  
15          Pittsburgh, PA 15213  
16          Phone: +1 (412) 268-2776  
17          Email: [jianma@cs.cmu.edu](mailto:jianma@cs.cmu.edu)

18 **Abstract**

19 The composition of the cell nucleus is highly heterogeneous, with different constituents forming com-  
20 plex interactomes. However, the global patterns of these interwoven heterogeneous interactomes remain  
21 poorly understood. Here we focus on two different interactomes, chromatin interaction network and  
22 gene regulatory network, as a proof-of-principle, to identify heterogeneous interactome modules (HIMs)  
23 in the nucleus. Each HIM represents a cluster of gene loci that are in spatial contact more frequently than  
24 expected and that are regulated by the same group of transcription factor proteins. We develop a new al-  
25 gorithm MOCHI to facilitate the discovery of HIMs based on network motif clustering in heterogeneous  
26 interactomes. By applying MOCHI to five different cell types, we found that HIMs have strong spatial  
27 preference within the nucleus and exhibit distinct functional properties. Through integrative analysis,  
28 this work demonstrates the utility of MOCHI to identify HIMs, which may provide new perspectives on  
29 3D genome organization and function.

30 **Introduction**

31 The cell nucleus is an organelle that contains heterogeneous components such as chromosomes, pro-  
32 teins, RNAs, and subnuclear compartments. These different constituents form complex organizations  
33 that are spatially and temporally dynamic [1, 2]. Interphase chromosomes are folded and organized in  
34 three-dimensional (3D) space by compartmentalizing the cell nucleus [3, 4], and different chromosomal  
35 loci also interact with each other [2]. The development in whole-genome mapping approaches such as  
36 Hi-C [5] to probing chromatin interactome has enabled comprehensive identification of genome-wide  
37 chromatin interactions, revealing important nuclear genome features such as loops [6, 7], topologically  
38 associating domains (TADs) [8, 9], and A/B compartments [5]. Nuclear genome organization has intri-  
39 cate connections with gene regulation [3, 10]. In particular, correlations between higher-order genome  
40 organization (including chromatin interactions and chromosome compartmentalization) and transcrip-  
41 tional activity have been demonstrated [6, 11, 12].

42 Systems level transcriptional machinery can often be represented by gene regulatory networks (GRNs),  
43 which are dynamic among various cellular conditions [13, 14]. GRN models the phenomena of selective  
44 binding of transcription factor (TF) proteins to *cis*-regulatory elements in the genome to regulate target  
45 genes [15, 16]. Transcription of co-regulated genes in GRN can be facilitated by long-range chromo-  
46 somal interactions [17] and chromatin interactome has been shown to exhibit strong correlations with  
47 GRN [18, 19]. Indeed, network-based representation of both chromatin interactome and GRN has been  
48 suggested to consider different subnuclear components holistically [20, 21]. The paradigm of viewing the  
49 nucleus as a collection of interacting networks among various constituents can potentially be extended to  
50 account for other types of related interactomes in the nucleus. However, whether these interactomes, in  
51 particular chromatin interactome and GRN, are organized to form functionally relevant, global patterns  
52 remains unknown.

53 In this work, as a proof-of-principle, we specifically consider two different types of interactomes in  
54 the nucleus: (1) chromatin interactome – a network of chromosomal interactions between different ge-  
55 nomic loci – and (2) a GRN where TF proteins bind to the genomic loci to regulate target genes’ transcrip-  
56 tion. Many studies in the past have analyzed the structure and dynamics of chromatin interactomes and

57 GRNs as well as the coordinated binding of transcription factors on folded chromatin [6, 7, 14, 22, 23].  
58 However, the global network level patterns between chromatin interactome and GRN are still unclear,  
59 and algorithms that can simultaneously analyze these heterogeneous networks in the nucleus to discover  
60 important network structures have not been developed.

61 Here we aim to identify mesoscale network structures where nodes of TFs (from GRN) and gene  
62 loci (from both chromatin interactome and GRN) cooperatively form distinct types of modules (i.e.,  
63 clusters). We develop a new algorithm, MOCHI (MOtif Clustering in Heterogeneous Interactomes),  
64 that can effectively uncover such network modules, which we call heterogeneous interactome modules  
65 (HIMs), based on network motif clustering using a 4-node motif specifically designed to reveal HIMs.  
66 Each identified HIM represents a collection of gene loci and TFs for which (1) the gene loci have higher  
67 than expected chromatin interactions between themselves, and (2) the gene loci are regulated by the same  
68 group of TFs. To demonstrate the utility of MOCHI to identify HIMs based on complex heterogeneous  
69 interactomes in the nucleus, we apply MOCHI to five different human cell types, identifying patterns of  
70 HIMs and their functional properties through integrative analysis. HIMs have the potential to provide  
71 new insights into the nucleome structure and function, in particular, the interwoven interactome patterns  
72 from different components of the nucleus. The source code of our MOCHI method can be accessed at:  
73 <https://github.com/ma-compbio/MOCHI>.

## 74 Results

### 75 Overview of the MOCHI algorithm

76 The overview of our method is illustrated in Fig. 1, with detailed algorithms described in the Methods  
77 section. Our goal is to reveal network clusters in a heterogeneous network such that certain higher-order  
78 network structures (e.g., the network motif  $M$  in Fig. 1A) are frequently contained within the same clus-  
79 ter. The input heterogeneous network in this work considers two types of interactomes: a GRN (directed)  
80 between TF proteins and target genes; and chromatin interaction network (undirected) between gene loci  
81 on the genome. For chromatin interactome, for each pair of gene loci within 10Mb, we use the “observed  
82 over expected” (O/E) quantity in the Hi-C data (we use O/E>1 as the cutoff in this work, but we found  
83 that our main results are largely consistent with different cutoffs; see Supplemental Information B.1) to  
84 define the edges in the chromatin interaction network. For GRN, we use the transcriptional regulatory  
85 networks from [14], which were constructed by combining enrichment of TF binding sites in enhancer  
86 and promoter regions and co-expression between TFs and genes. If a TF protein regulates a gene, we  
87 add a directed edge from the TF to the gene. We then merge the chromatin interaction network and the  
88 GRN from the same cell type to form a network  $G$  with nodes that are either TF proteins or gene loci  
89 together with the directed and undirected edges defined above (Fig. 1B).

90 We specifically consider the network motif  $M$  which has four nodes, i.e., two gene loci and two  
91 TFs in the heterogeneous network with two genes whose genomic loci are spatially more proximal to  
92 each other (than expected) within the nucleus and that are also co-regulated by the two TFs (Fig. 1A)  
93 (see the Methods section and Supplemental Information for the justification of this motif). Our goal  
94 is to reveal higher-order network clusters based on this particular network motif. In other words, we  
95 want to partition the nodes in the network such that this 4-node network motif occurs mostly within the  
96 same cluster. Based on the motif, our MOCHI algorithm, which extends the original algorithm in [24],

97 constructs an undirected, weighted network  $G_M$  (Fig. 1D) based on subgraph adjacency matrix  $W_M$   
98 (Fig. 1C). We then apply recursive bipartitioning in  $G_M$  to find multiple clusters (Fig. 1E). We call such  
99 clusters HIMs, which, in this work, represent network structures containing the same group of TFs that  
100 regulate many target genes whose spatial contact frequencies are higher than expected. Since TFs can  
101 regulate multiple sets of genes that may belong to different clusters, different HIMs may overlap by  
102 sharing TFs. The algorithm details of MOCHI are in the Methods section.

### 103 **MOCHI identifies HIMs in multiple cell types**

104 We applied MOCHI to five different human cell types: GM12878, HeLa, HUVEC, K562, and NHEK.  
105 The input heterogeneous network of each cell type has 591 TFs, ~12,000 expressed genes, and ~1  
106 million regulatory interactions (Table S1). A few examples of HIMs identified in GM12878 are shown  
107 in Fig. 1F-H, including overlapping HIMs in Fig. 1H. We found that the identified HIMs in five cell types  
108 share several basic characteristics. The number of identified HIMs ranges from 650 to 806 in different  
109 cell types, with at least 71.9% of the HIMs sharing TFs with other HIMs in each cell type. Notably, HIMs  
110 cover a majority (62.1-77.2%) of the genes in the heterogeneous networks (Table S1). For example, in  
111 GM12878, there are 591 TFs co-regulating 7,617 (69.1%) genes in 650 HIMs. The HIMs have, on  
112 average, 9-17 TFs regulating 9 genes in different cell types (Table S2). In addition, we found that the  
113 identified HIMs in different cell types share similar connections to 3D genome features (Supplemental  
114 Information B.3, Table S2).

115 To further assess that the genes in a HIM are indeed co-regulated by the same TF, we used the  
116 available ChIP-seq data of 26 TFs in GM12878 and K562 cells from the ENCODE project [25]. We  
117 found that for all the HIMs in GM12878 or K562 with these 26 TFs, more than half (55.85%) of them  
118 have  $\geq 50\%$  of their genes with corresponding TF ChIP-seq peaks within 10kb of the transcription start  
119 site, further suggesting that the genes in HIMs identified by MOCHI share regulatory TFs. In addition,  
120 MOCHI can reliably identify HIMs with different parameters in various cell types (Supplemental Infor-  
121 mation B.1). Importantly, we justified the choice of the 4-node motif  $M$  by showing its advantages over  
122 a triangle motif and a bifan motif (Supplemental Information B.2). The triangle and bifan motifs do not  
123 explicitly encode the co-regulation between TFs and the spatial proximity between genes. These results  
124 demonstrate that MOCHI can reliably identify HIMs across multiple cell types.

### 125 **HIMs show strong preference in spatial location relative to subnuclear structures**

126 Next, we specifically analyzed the spatial localization of HIM in the nucleus. Recently published SON  
127 TSA-seq and Lamin B TSA-seq datasets quantify cytological distance of chromosome regions to nuclear  
128 speckles and nuclear lamina, respectively [12]. In K562, which is currently the only cell type with  
129 TSA-seq data, 60.7% of the HIMs have mean SON TSA-seq score higher than 0.284 (80-th percentile  
130 of the SON TSA-seq score), suggesting that the genes in these HIMs, on average, are within 0.518 $\mu$ m  
131 (estimated in [12]) of nuclear speckles (Fig. 2A). Compared to the genes in the K562 heterogeneous  
132 network but not assigned to HIMs, the genes in HIMs have higher SON TSA-seq score and lower Lamin  
133 B TSA-seq score ( $p < 2.22e-16$ ; Fig. S1).

134 We specifically looked at the HIMs that are away from the nuclear interior. Fig. 2B shows one HIM  
135 (#541) that is close to nuclear lamina (mean Lamin B TSA-seq score 0.593, mean SON TSA-seq score  
136 -0.642). This HIM has 9 TFs co-regulating 6 genes that span 6.78 Mb on chromosome 3. The Hi-C edge  
137 density (see Supplemental Information A.4) among these genes is 0.667, suggesting that these 6 genes

138 as a group are spatially closer to each other than expected (i.e., connected with chromatin interaction).  
139 The SON TSA-seq scores of the 6 genes are low but tend to be the local maxima (i.e., small peaks within  
140 valleys), while the Lamin B TSA-seq scores are high but tend to be the local minima (i.e., small valleys  
141 within peaks), suggesting that these gene loci are localized more towards the nuclear interior than their  
142 surrounding chromatin. Five out of the 6 genes are expressed with FPKM $\geq$ 3.4. The gene RPL15 in  
143 this HIM is a K562 essential gene [26]. The TF proteins CDX1, HOXA9, and HOXA10 are involved in  
144 leukemia and hematopoietic lineage commitment provided by Genecards [27]. This suggests that even  
145 though HIM #541 is a HIM away from nuclear speckle, it may play relevant functional roles in K562.

146 Recently, Quinodoz et al. [28] reported that inter-chromosomal interactions are clustered around two  
147 distinct nuclear bodies as hubs, including nuclear speckles and nucleoli. By comparing with the genomic  
148 regions organized around nucleolus based on data from the SPRITE method in GM12878 [28], we found  
149 that vast majority (85.4%) of the GM12878 HIMs do not have genes close to the nucleolus. Earlier work  
150 estimated that only 4% of the human genome is within nucleolus-associated domains [29]. It is therefore  
151 expected that only a small number of HIMs would be close to the nucleolus. Indeed, we found that there  
152 are only 30 (4.62%) GM12878 HIMs with all their genes near the nucleoli. Notably, 16 out of these 30  
153 HIMs have at least one TF protein located close to nucleoli according to protein subcellular locations  
154 from the human protein atlas [30]. For example, HIM #267 has 4 TF regulators: ETS1, ETV6, PPARG,  
155 and PTEN, where ETV6 is known to localize to the nucleoli.

156 Earlier work from Hi-C data showed that at megabase resolution the interphase chromosomes are seg-  
157 regated into A and B compartments that are largely active and inactive in transcription, respectively [5].  
158 Chromosome regions in B and A compartments have nearly identical agreements with lamina associated  
159 domains (LADs) and inter-LADs (i.e., more towards interior) [4]. Compartment A regions also replicate  
160 earlier than compartment B regions [31]. We found that the genes in HIMs are preferentially in A com-  
161 partments and replicated earlier across cell types. Specifically, 57.4% of HIMs have genes that are all in  
162 A compartments in K562. Only a small proportion (4.49%) of HIMs have over 50% of genes in B com-  
163 partments (Fig. 2C). We found that the genes in HIMs as a whole are more enriched in A compartments,  
164 with 89.1% of them in A compartments ( $p < 2.22e-16$ , hypergeometric test; Fig. 2D). Compartment A  
165 can be further subdivided into A1 and A2 subcompartments in GM12878 [6] at a finer scale. Among  
166 the 369 GM12878 HIMs with genes all in A compartments, 198 (53.66%) HIMs have  $\geq 80\%$  of their  
167 genes in A1 subcompartments, 60 (16.26%) HIMs are in A2 subcompartments, and the rest 111 HIMs  
168 span both A1 and A2 compartments. Additionally, we found that the genes assigned to HIMs have much  
169 earlier replication timing than the other genes ( $p < 2.22e-16$ ; Fig. 2E). We also observed that the genes on  
170 the same chromosome that are in HIMs tend to have more similar replication timing as compared to the  
171 genes (on the same chromosome) that are not in HIMs (Fig. S2). These patterns can also be observed in  
172 other cell types (Fig. S2).

173 Taken together, these results suggest that HIMs have strong preference to localize towards the nuclear  
174 interior in active compartments with the majority of them being in proximity of the nuclear speckles and  
175 replicating earlier.

## 176 **HIMs are enriched with essential genes, super-enhancers, and PPIs**

177 Next, we explored the functional properties of HIMs. We again grouped the genes assigned to HIMs  
178 into one set and the genes in the heterogeneous network but are not assigned to HIMs into another set.  
179 For a fair comparison, we also stratify the gene sets by chromosome number. We call these clusters

merged-HIM clusters and non-HIM clusters accordingly. We first compared with the information of gene essentiality [26] (see Supplemental Information A.5). We found that genes assigned to HIMs are enriched with essential genes across all five cell types. For example, 12.7% of the genes assigned to HIMs in K562 are K562 essential genes, which is significantly higher than the proportion (7.79%) of the genes not assigned to HIMs ( $p=1.13e-12$ ; Fig. 3A). This observation is also present across chromosomes (Fig. S3A). Across the cell types, genes assigned to HIMs consistently have higher proportions of essential genes than genes not assigned to HIMs ( $p\leq2.17e-6$ ; Fig. S3B). Regarding gene expression level, we found that genes assigned to HIMs are more highly expressed and expressed at similar levels (Fig. 3B, Fig. S4).

Super-enhancers are known to be associated with many cell type-specific functions [32]. To study the connections between HIMs and super-enhancers, we computed the cluster-size normalized number of super-enhancers annotated in [32] that (1) have Hi-C contacts with, and (2) are close to (window size=50kb) at least one gene in each cluster. We found that HIMs are enriched with spatial contacts with super-enhancers. Specifically, the merged-HIMs have at least 6-fold higher normalized number of super-enhancers than the non-HIMs across cell types (Fig. 3C, Fig. S5). The significant pattern is consistent with a varied window size from 20kb to 1Mb (Fig. S5).

Protein-protein interactions (PPIs) can further stabilize TF-DNA binding of the interacting TFs [16]. We ask whether TFs in the same HIM tend to have more PPIs with each other. We computed the density of the sub-PPI network induced by the TFs in a HIM, where the PPI network is based on 591 TF proteins used in this study (see Supplemental Information A.5). We found that TFs within HIMs are enriched with PPIs among themselves as compared to random cases selected from the 591 TFs. For example, in GM12878, TFs NR3C1 and TFEB, which are master regulators [32], co-regulate 8 genes with the other 7 TFs proteins in a HIM (Fig. 3D). This particular sub-PPI network of the 9 TFs has 14 interactions. The density of this sub-PPI network is 0.389 which is 2.46 times higher than the average density (0.158) of the random cases. Overall, the median density of the sub-PPI networks induced by TFs in the identified HIMs in GM12878 is 0.214, much higher than the random cases ( $p<2.22e-16$ ; Fig. 3E). This observation is also consistent in other cell types in this study (Fig. S6). We also found that the significance is not affected by a varied number of TFs across HIMs (Fig. S6).

These results suggest that the genes and TFs involved in HIMs likely perform critical roles, which are manifested by the level of gene essentiality of target genes, engagement of super-enhancers, and enrichment of PPI among TFs.

## Genes in HIMs exhibit stability and variability across cell types

To study how HIMs change across different cell types, we first focused on the assignment of genes to HIMs in different cell types. Through pairwise comparison, we found that the genes assigned to HIMs have the highest degree of overlap between GM12878 and K562 as compared to the other cell types, which is consistent with the fact that both GM12878 and K562 are from human hematopoietic cells (Fig. S7A). Comparisons among all five cell types showed that 3,025 genes are consistently assigned to HIMs, accounting for 30.91% to 40.06% of genes that are in the HIMs in each cell type (Fig. 4A). In contrast, only a small fraction ( $\leq5.93\%$ ) of genes are uniquely assigned to the HIMs in each cell type. For example, out of the 8,034 genes in the GM12878 HIMs, only 344 (4.28%) genes are not assigned to HIMs in other cell types (Fig. 4A).

The genes consistently and uniquely assigned to HIMs are enriched with distinct functional terms

222 using DAVID [33] (Table S5). The genes consistently assigned to HIMs are strongly enriched with  
223 functions related to essential cellular machinery, whereas the genes uniquely assigned to HIMs in a  
224 particular cell type are enriched with more cell type-specific functions. An example is NHEK HIM #107  
225 (Fig. 4B). Among the 6 genes in this HIM, DSC1, DSC3, DSG1 are not assigned to HIMs in the other  
226 cell types. These 6 genes are involved in the keratinization pathway based on GeneCards [27]. We  
227 further assessed the assignment of housekeeping genes [34] and essential genes to HIMs. We found that  
228 for both sets of genes, the majority ( $\geq 84\%$ ) of them are assigned to HIMs consistently or in at least 3 out  
229 of the 5 cell types (Fig. 4C), suggesting that the genes with crucial functions tend to form spatial clusters  
230 across multiple cell types.

231 We next analyzed the variability of HIMs in terms of spatial proximity to subnuclear compartments.  
232 We found that 15 out of the 30 HIMs close to nucleoli in GM12878 (based on the data from [28]) have  
233 mean SON TSA-seq score  $\geq 0.284$  in K562 (based on the data from [12]) (Fig. 4D), in other words, these  
234 HIMs are involved in a change of spatial position from nucleoli to speckle between GM12878 and K562.  
235 One notable example is HIM #267 in GM12878 which has the highest mean SON TSA-seq score (2.41)  
236 in K562. Interestingly, the 10 genes (in HIM #267 in GM12878) together with another 8 genes form a  
237 new HIM (#628) in K562. This GM12878 HIM #267 has four TFs: ETS1, ETV6, PPARG, and PTEN.  
238 On the other hand, the K562 HIM #628 has four different TFs: KLF4, NFKB1, STAT3, and WT1, where  
239 KLF4, STAT3, and WT1 are known to be involved in the progression of leukemia.

240 To compare the detailed membership changes of HIMs across cell types, we computed Jaccard in-  
241 dices, denoted by  $J_{TF}$  and  $J_{gene}$ , of the TF members and gene members between HIMs from two  
242 different cell types, respectively. We found that the gene members undergo a moderate change from  
243 one cell type to another, whereas the TF members change at a much higher rate.  $J_{gene}$  has a median of  
244 0.096 and it is higher than expected  $J_{gene}$  between random gene sets while controlling the set size and  
245 chromosome number (median ratio=14.12, Fig. 4E). On the other hand,  $J_{TF}$  has a median of 0.017 and  
246 it is close to expected  $J_{TF}$  between randomly selected control TF sets (median ratio=0.878, Fig. 4E).  
247 There are at least two phenomena jointly contributing to these observations. First, the Hi-C interaction  
248 networks and GRNs are highly cell type-specific, as 66% Hi-C interactions and 31.4% GRN interactions  
249 only exist in one cell type (Table S3). Second, given a HIM identified in a cell type, the motif  $M$  density  
250 of the HIM (see Supplemental Information A.4) has higher fold change than the Hi-C edge density of  
251 the HIM in another cell type ( $p < 2.22e-16$ ; Fig. 4F). In other words, the co-regulation relationships of the  
252 TFs on the genes in HIMs change more often across cell types than the spatial proximity relationships  
253 between the gene loci. However, we observed that if HIMs from two different cell types share a higher  
254 number of housekeeping genes, they tend to have a higher  $J_{TF}$  (Fig. 4G). We found a similar pattern for  
255 essential genes (Fig S7B).

## 256 **Conserved and cell type-specific HIMs have distinct properties**

257 Motivated by the gene membership dynamics of HIMs across cell types, we further classified HIMs into  
258 conserved and cell type-specific HIMs. For HIMs in a given cell type, we call a HIM conserved if it  
259 shares a significantly high proportion of genes ( $J_{gene} \geq 1/3$ ,  $p \leq 0.001$ , Bonferroni adjusted hypergeo-  
260 metric test) with at least one HIM in other cell types (i.e., the HIM is recurrent). Note that  $J_{gene} \geq 1/3$   
261 represents that two equal-sized gene sets share more than half of their genes. The rest are called cell type-  
262 specific HIMs. As a result, 40.69-47.38% of the identified HIMs in each cell type are cell type-specific  
263 HIMs. Fig. 5 shows a cell type-specific HIM, HIM #712, in K562 and its changes in other cell types.

264 This HIM covers 9 genes on chromosome 11. These genes spatially contact each other at higher frequencies  
265 than expected (Fig. 5A) and are co-regulated by TF protein BCL6B and CPEB1 in K562 (Fig. 5B).  
266 In other cell types, at most 4 out of the 9 genes are assigned to HIMs (Fig. 5C). We found that this HIM  
267 has K562-specific chromosomal structures and functional annotations. The genomic region covering  
268 the genes in the HIM is in A compartment in K562 but switches to B compartment in other cell types  
269 (Fig. 5D). One nearby upstream region is annotated as a super-enhancer only in K562 [32] (Fig. 5E).  
270 Many sites are annotated as transcriptionally active states, such as enhancers, promoters, or transcribed  
271 states in K562, but not in other cell types based the results from ChromHMM [35] (Fig. 5F). The genes  
272 MRPL16, OSBP, and PATL1 are essential genes in K562. This example demonstrates that the K562-  
273 specific HIM has specific chromatin organization and biological functions.

274 Overall, we found that the conserved and cell type-specific HIMs have distinct properties of in-  
275 teractomes across cell types. Compared to cell type-specific HIMs, conserved HIMs exhibit stronger  
276 clustering features with higher Hi-C edge density, higher GRN edge density, and higher motif  $M$  density  
277 ( $p \leq 8.15e-4$ ; Fig. S8). Also, conserved HIMs tend to be closer to the nuclear interior with a higher pro-  
278 portion of their genes in A compartment, and their genes replicate earlier and synchronously (Fig. S8).  
279 Moreover, we found that conserved HIMs and cell type-specific HIMs tend to have large differences  
280 in gene expression level and cell type-specific genes. The conserved HIMs have higher mean gene ex-  
281 pression level than the cell type-specific HIMs in 3 cell types except for NHEK and HUVEC ( $p < 0.05$ ;  
282 Fig. S9). On the other hand, cell type-specific HIMs have a higher proportion of cell type-specific genes  
283 ( $p \leq 0.02$ ; see Supplemental Information A.5) than conserved HIMs across five cell types (Fig. S9). Taken  
284 together, our results demonstrate that conserved and cell type-specific HIMs, in general, have distinct  
285 network properties, spatial location preference, and functional characteristics.

## 286 Discussion

287 To better understand the heterogeneous nature of different components in the nucleus, new computa-  
288 tional models are needed to consider different types of molecular interacting networks. In this work, we  
289 developed MOCHI to specifically consider two types of different interactomes in the cell nucleus: (1)  
290 a network of chromosomal interactions between different gene loci, and (2) a GRN where TF proteins  
291 bind to the genomic loci to regulate target genes. MOCHI is able to identify network structures where  
292 nodes of TFs (from GRN) and gene loci (from both chromatin interactome and GRN) cooperatively  
293 form distinct network clusters, which we call HIMs, by utilizing a new motif clustering framework for  
294 heterogeneous networks. To the best of our knowledge, this is the first algorithm that can simultane-  
295 ously analyze these heterogeneous networks within the nucleus to discover important network structures  
296 and properties. By applying MOCHI to five different human cell types, we made new observations to  
297 demonstrate the biological relevance of HIMs in 3D nucleome.

298 Our method has multiple methodological contributions. We further extended the motif conductance  
299 clustering method [24] to find overlapping HIMs in heterogeneous networks. Our study shows the util-  
300 ity of our new algorithm to identify HIMs based on complex heterogeneous molecular interactomes. In  
301 addition, our method can be further modified to identify other types of potentially interesting HIMs in  
302 heterogeneous networks by replacing the 4-node motif  $M$  with relevant motifs, especially when addi-  
303 tional types of interactomes are included. For example, in addition to considering chromatin interactions  
304 and protein-DNA interactions as we did in this work, it would be of interest to incorporate other types of

305 relevant interactomes in the nucleus, such as the RNA-chromatin interactome [36].

306 How can we explain the formation of HIMs? In Fig. 6, we illustrate a possible model of HIMs within  
307 the nucleus. HIMs (light pink domains) are toward the interior with a group of interacting TFs and chro-  
308 matin loci. The set of TFs in a HIM cooperatively regulate target genes, which also have higher contact  
309 frequency than expected. Note that this is conceptually consistent with recently reported co-localization  
310 of TF pairs [22]. Some of these TF clusters may be related to the localization preferences of TF proteins  
311 in nuclear compartments, such as nuclear speckles that are enriched with various transcriptional activ-  
312 ities [12, 37]. Indeed, we found that the majority of the identified HIMs are close to nuclear speckles.  
313 The definitions of HIMs may also have intrinsic connections with the emerging findings on the mech-  
314 anism of nuclear subcompartment formation, where TFs and their potential regulating genes/chromatin  
315 are trapped by localized liquid-like chambers through the phase separation [38, 39]. Evidence has been  
316 shown that phase separation can help explain the formation of super-enhancer mediated gene regula-  
317 tion [39, 40]. From our analysis, we found that genes assigned to HIMs are enriched with contacts  
318 with super-enhancers. The genes consistently assigned to HIMs are enriched with essential biologi-  
319 cal processes related to chromosomal organization and transcription. However, the detailed formation  
320 mechanisms for HIMs, which may involve both *cis* elements and *trans* factors, remain to be investigated.  
321 It would also be important to delineate the different roles of both different TFs and different genes in  
322 forming the HIMs, as some of them may be necessary and others may be redundant for the stability of  
323 HIMs. In addition, more experimental data are needed to further evaluate the functional significance  
324 of HIMs. For example, although we observed connections between HIMs and 3D genome organization  
325 features, the intricate functional relevance among these different higher-order nucleome units that jointly  
326 contribute to gene regulation in different cellular conditions is yet to be revealed. Nevertheless, HIMs  
327 may become a useful type of nuclear genome unit in integrating heterogeneous nucleome mapping data,  
328 which has the potential to provide new insights into the interplay among different constituents in the  
329 nucleus and their roles in 3D nucleome structure and function.

330 **Methods**

331 **Brief introduction to homogeneous network clustering by motif conductance**

332 We first review higher-order network clustering method that can identify a cluster of nodes  $S$  based on  
 333 motif conductance (defined below). We then introduce our algorithm MOCHI in the next subsection. Let  
 334  $G$  be an undirected graph with  $N$  nodes and  $A$  be the adjacency matrix of  $G$ .  $[A]_{ij} \in \{0, 1\}$  represents  
 335 the connection between nodes  $i$  and  $j$ . The *conductance* of a cut( $S, \bar{S}$ ), where  $S$  is a subset of the nodes  
 336 is defined as:

$$\varphi_G(S) = \frac{\text{cut}_G(S, \bar{S})}{\min[\text{Vol}_G(S), \text{Vol}_G(\bar{S})]}, \quad (1)$$

337 where  $\text{cut}_G(S, \bar{S}) = \sum_{i \in S, j \in \bar{S}} [A]_{ij}$  is the number of edges connecting nodes in  $S$  and  $\bar{S}$ .  $\text{Vol}_G(S) =$   
 338  $\sum_{i \in S} \sum_{j=1}^N [A]_{ij}$  is the sum of the node degree in  $S$ . Moreover, the conductance of the graph  $G$ ,  $\varphi^G$ ,  
 339 is defined as  $\min_S \varphi_G(S)$ . The  $S$  that minimizes the function is the optimal solution. Finding the  
 340 optimal  $S$  is NP-hard, but spectral methods such as Fiedler partitions can obtain clusters effectively [41].  
 341 Recently, the conductance metric is generalized to motif conductance [24, 42], where a motif refers to  
 342 an induced subgraph. The motif conductance computes  $\text{cut}_G(S, \bar{S})$  and  $\text{Vol}_G(S)$  based on a chosen  $n$ -  
 343 node motif. When  $n = 2$ , the motif is an interaction that reduces the motif conductance to conductance  
 344 in Eq. (1). When  $n \geq 3$ , the motif conductance may reveal new higher-order organization patterns  
 345 of the network [24]. A more recent network clustering method that incorporates network higher-order  
 346 structures has been developed in the setting of hypergraph clustering [43], which includes the motif  
 347 conductance as a special case. However, one key limitation of the aforementioned methods is that they  
 348 cannot identify overlapping clusters, which is a crucial feature of the heterogeneous networks that we  
 349 want to achieve in this work.

350 **MOCHI – Higher-order network clustering to identify HIMs in a heterogeneous network**

351 We developed a higher-order network clustering method based on network motif to identify overlapping  
 352 HIMs in a heterogeneous network by extending the approach in [24]. We call our method MOCHI  
 353 (MOtif Clustering in Heterogeneous Interactomes). We illustrate the workflow of MOCHI in Fig. 1.  
 354 First, we select a specific heterogeneous 4-node network motif  $M$  (Fig. 1A). In  $M$ , two nodes are TFs  
 355 and the other two nodes are genes. Both TFs regulate the two genes and the two genes are spatially  
 356 more proximal to each other than expected. The motivation for choosing the subgraph  $M$  is that it is  
 357 the building block of HIMs given that our goal is to discover a group of genes that contact with each  
 358 other more frequently than expected and are regulated by the same set of TFs. As compared to simpler  
 359 motifs (e.g., 3-node motif where one node is TF), our 4-node motif defined here has the advantage of  
 360 simultaneously considering a pair of genomic loci that interact with each other higher than expected and  
 361 that are co-regulated by the same pair of TFs.

362 Conceptually, our method searches for HIMs with two goals. The TFs and genes in the same HIM  
 363 should be involved in many occurrences of  $M$ . Additionally, HIM should avoid cutting occurrences of  
 364  $M$ , where a cut of occurrences of  $M$  means that only a subset of TFs and genes in the occurrences of  
 365  $M$  are in the HIM node set. More formally, our method aims to find HIMs with the node set  $S$  that  
 366 minimizes the motif conductance

$$\varphi_M(S) = \frac{\text{cut}_M(S, \bar{S})}{\min[\text{Vol}_M(S), \text{Vol}_M(\bar{S})]}. \quad (2)$$

367 We first introduce some notations before we explain  $\varphi_M(S)$ . Let  $G$  be the given heterogeneous  
 368 network (e.g., Fig. 1B). Let  $\mathbb{M}$  be the set of occurrences of the motif  $M$  in  $G$ . For simplicity and without  
 369 confusion, we also denote an occurrence of the motif  $M$  as  $M$ . Let  $V_M$  be the vertex set of the 2 TFs and  
 370 2 genes in  $M \in \mathbb{M}$ . In Eq. (2),  $\text{cut}_M(S, \bar{S})$  is the number of occurrences of the subgraph  $M$  that are cut  
 371 by  $S$ . Formally,

$$\text{cut}_M(S, \bar{S}) = \sum_{M \in \mathbb{M}} \mathbb{1}(|V_M \cap S| \in \{1, 3\}) + \alpha \sum_{M \in \mathbb{M}} \mathbb{1}(|V_M \cap S| = 2), \quad \alpha > 1, \quad (3)$$

372 where  $\mathbb{1}$  is an indicator function. Here,  $\text{cut}_M(S, \bar{S})$  distinguishes the number of nodes of the 4-node  
 373 motif  $M$  being assigned to  $S$  and  $\bar{S}$ . Specifically, it adds a higher penalty for the cut to the cases where  
 374 two nodes in  $M$  are assigned to  $S$  and two nodes are assigned to  $\bar{S}$ , as compared to the case where one  
 375 node or three nodes are assigned to  $S$ , by letting  $\alpha > 1$  in Eq. (3). This is because the 1-vs-3 split could  
 376 still keep interaction information from both GRN and chromatin interaction network, and the 2-vs-2 split  
 377 will lose either of the information. We show that when  $\alpha = 4/3$  in Eq. 3 the clustering results would be  
 378 near optimal (Supplemental Information A.3). Thus,  $\alpha$  is set to 4/3 in this paper.  $\text{Vol}_M(S)$  is the number  
 379 of nodes in the occurrences of  $M$  that are in  $S$ , which is defined as:

$$\text{Vol}_M(S) = \sum_{i \in S} \sum_{M \in \mathbb{M}} \mathbb{1}(i \in V_M). \quad (4)$$

380 Similarly, we define the subgraph conductance of the graph  $G$  based on motif  $M$ ,  $\varphi_M^G$  as  $\min_S \varphi_M(S)$ .  
 381 In the following procedures of the algorithm, we show that the motif conductance is equivalent to the  
 382 normal conductance in a projection of the graph by calculating the subgraph adjacency matrix. Thus,  
 383 finding the set  $S$  that achieves the minimum subgraph conductance is also NP-hard, following that it is  
 384 NP-hard to find the minimal  $\varphi_G(S)$ . We describe our algorithm MOCHI to find HIMs that approximate  
 385 the solution.

### 386 1 – Calculate subgraph adjacency matrix $W_M(G)$

387 We first calculate the subgraph adjacency matrix  $W_M(G)$  by

$$[W_M(G)]_{ij} = \sum_{M \in \mathbb{M}} \mathbb{1}(i \in V_M, j \in V_M), \quad (5)$$

388 where  $[W_M(G)]_{ij}$  is the number of occurrences of the subgraph  $M$  in  $G$  that cover both  $i$  and  $j$  (see  
 389 example in Fig. 1C). For example, if both  $i$  and  $j$  are TFs,  $[W_M]_{ij}$  reflects the number of paired gene loci  
 390 that are spatially more proximal to each other than expected and that are also co-regulated by TFs  $i$  and  
 391  $j$ . If both  $i$  and  $j$  are genes,  $[W_M]_{ij} = 0$  if  $i$  and  $j$  are not more spatially proximal to each other than  
 392 expected. Otherwise,  $[W_M]_{ij}$  is the number of paired TFs that co-regulate  $i$  and  $j$ . Generally,  $W_M(G)$  is  
 393 symmetric and  $[W_M(G)]_{ij} \geq 0$ . Thus  $W_M(G)$  can be viewed as the adjacency matrix of an undirected  
 394 weighted network. Let  $G_M$  denote the network with  $W_M(G)$  as the adjacency matrix (see Fig. 1D for  
 395 example). It is important to note that there are genes or TFs that may not be in any occurrence of  $M$ ,  
 396 which would lead to zero vectors in the corresponding rows and columns in  $W_M(G)$ . These singleton  
 397 nodes in  $G_M$  would be removed before the next step.

398 **2 – Apply Fiedler partitions to find a cluster in  $G_M$**

399 We utilize Fiedler partitions similar to the algorithm in [24] to find a cluster  $S$  in graph  $G_M$ , where  
400  $\varphi_{G_M}(S)$  is close to the global optimal conductance of the graph:  $\varphi(G_M)$ . Recall that  $\varphi(G_M)$  is the  
401 minimum of  $\varphi_{G_M}(S_1)$  over all possible sets  $S_1$ . The method is described as follows:

- Calculate the normalized Laplacian matrix of  $W_M(G)$ :

$$\mathcal{L} = \mathcal{I} - D_{G_M}^{-1/2} W_M(G) D_{G_M}^{-1/2}, \quad (6)$$

403 where  $\mathcal{I}$  is a identity matrix,  $D_{G_M}$  with  $[D_{G_M}]_{ii} = \sum_{j=1}^N (W_M(G))_{ij}$  is the diagonal degree matrix  
404 of  $G_M$ .

- Calculate the eigenvector  $v$  of the second smallest eigenvalue of  $\mathcal{L}$ .
- Find the index vector  $(\alpha_1, \dots, \alpha_N)$ , where  $\alpha_k$  is the  $k$ -th smallest value of  $D_{G_M}^{-1/2}v$ .
- $S = \underset{1 \leq k \leq N}{\operatorname{argmin}} \varphi_{G_M}(S_k)$ , where  $S_k = \{\alpha_1, \dots, \alpha_k\}$ .

408 The sets  $S$  and  $\bar{S}$  are two disjoint clusters for the heterogeneous network  $G$ .

409 **3 – Apply recursive bipartitioning to find multiple HIMs**

410 We then utilize recursive bipartitioning to find multiple HIMs. We use a very different strategy than the  
411 one in [24] to select which cluster to split at each iteration, in order to specifically allow overlapping  
412 motif clusters (HIMs) with shared TFs. At each iteration, we split one HIM into 2 child HIMs. After  
413 iteration  $\ell - 1$ , there are  $\ell$  HIMs:  $S_1, S_2, \dots, S_\ell$ .

414 At next iteration  $\ell$ , one HIM  $S_k$  is selected if the graph it forms,  $G_k$ , has the lowest subgraph con-  
415 ductance value  $\varphi_M^{G_k}$  among  $\varphi_M^{G_j}$ ,  $1 \leq j \leq \ell$ . We set a threshold  $t_1$  for  $\varphi_M^{G_k}$ . If  $\varphi_M^{G_k} \leq t_1$ ,  $S_k$  will be  
416 split into two child HIMs  $S_k(c)$  and  $\overline{S_k(c)}$  by treating the induced heterogeneous subnetwork as a new  
417 network  $G_k$  and repeating Steps (1) and (2) for graph  $G_k$ . However, if the partition of graph  $G_k$  would  
418 lead to zero motif occurrence in either of its child graphs, we would stop partitioning this graph, add a  
419 large enough penalty value to its conductance value (to make sure it would not be selected to partition  
420 again), and move on to the next iteration. Otherwise, when  $\varphi_M^{G_k} > t_1$ , the recursive bipartitioning process  
421 will stop as all the HIM's subgraph conductance value passes the threshold.

422 **4 – Find overlapping HIMs**

423 Finally, we reconcile the HIMs from the clustering history tree to find overlapping HIMs. This step is  
424 added because the HIMs after Step (3) share no TFs. To reconcile the results, we first trace back the  
425 ancestral HIMs up to certain generations for each HIM based on the conductance value of its ancestor  
426  $\varphi_M^{G_{anci}}$ , where  $i = \{1, 2, 3, \dots\}$  denotes for the ‘parent’, ‘grandparent’ of the HIM. We trace along the  
427 tree until  $\varphi_M^{G_{anci}} \leq t_2$ , where  $t_2$  denotes another threshold. Clearly,  $t_2$  has to be smaller than  $t_1$  to  
428 make this process practical. Next, we pool together the TFs from the HIM and from its ancestor HIMs.  
429 We sequentially remove pooled TFs from the HIM according to their contribution to the number of  
430 occurrences of the subgraph  $M$  based on the graph this HIM represents, and stop this process when  
431 removing certain TF would cause a large decrease in the number of subgraphs.

432 **Pseudocode and complexity of our algorithm**

433 The pseudocode of our MOCHI algorithm is presented in the Supplemental Information A.1. The run-  
434 time of the algorithm is  $O(t^2 c^2)$ , where  $t$  and  $c$  ( $t \ll c$ ) are the number of TFs and the number of gene loci  
435 in the input heterogeneous network, respectively (detailed analysis in Supplemental Information A.2).

436 **Summary of the algorithm**

437 Given a heterogeneous network from chromatin interactome network and GRN, our algorithm MOCHI  
438 will identify multiple and overlapping HIMs, which represent clusters of genes and TFs where the genes  
439 are interacting more frequently than expected and are also co-regulated by the same set of TFs. MOCHI  
440 has a few key differences as compared to the subgraph conductance method in [24]. First, the input of our  
441 algorithm is a heterogeneous network with different types of nodes (TFs and gene loci), which are treated  
442 differently, while the input network for the method in [24] is rather homogeneous. Second, the algorithm  
443 in [24] will not explicitly identify multiple overlapping clusters. In MOCHI, we further developed a  
444 recursive bipartitioning method to find multiple HIMs that may overlap. Specifically, we selected a HIM  
445 to split if it has the smallest motif conductance among the HIMs at each interaction. In other words, we  
446 split the HIM that has the clearest pattern of multiple clusters. HIMs with overlapping TFs will be split  
447 in the late stage of iterations, and the overlapping information is encoded in the clustering history tree.

448 The recent method on hypergraph clustering [43] can be applied to identify non-overlapping HIMs  
449 where a hyperedge is defined as the motif  $M$ . However, similar to the method in [24], it was not designed  
450 to identify overlapping clusters, i.e., the method would not be able to find multiple overlapping HIMs  
451 that we would need. Our method also has clear differences as compared to previous works on multi-layer  
452 network clustering (see review in [44]). First, the inputs are different. A multi-layer network typically  
453 has only one type of nodes and different types of interactions connecting nodes within the same layer and  
454 between layers. The heterogeneous network in this work has different types of nodes (TF proteins and  
455 gene loci) and also edges. Previous multi-layer network clustering methods are not directly applicable  
456 to identify HIMs. Second, the outputs are different. The majority of multi-layer network clustering  
457 methods aim to find clusters that are either consistently observed across multiple layers or observed only  
458 in a specific layer, which are conceptually different from HIMs.

459 **Acknowledgement**

460 This work was supported in part by the National Institutes of Health Common Fund 4D Nucleome  
461 Program grant U54DK107965 (J.M.), National Institutes of Health grant R01HG007352 (J.M.), and  
462 National Science Foundation grant 1717205 (J.M.). The authors would like to thank Bas van Steensel  
463 and members of Jian Ma's laboratory (Ben Chidester, Tianming Zhou, Kyle Xiong, and Yang Yang) for  
464 helpful comments to improve the manuscript.

465 **Author Contributions**

466 Conceptualization, J.M.; Methodology, D.T., R.Z., and J.M.; Software, D.T., R.Z.; Investigation, D.T.,  
467 R.Z., Y.Z., X.Z., and J.M.; Writing – Original Draft, D.T., R.Z., and J.M.; Writing – Review & Editing,  
468 D.T. and J.M.; Funding Acquisition, J.M.

469 **Declaration of Interests**

470 The authors declare no competing interests.

471 **References**

- 472 [1] Christian Lanctôt, Thierry Cheutin, Marion Cremer, Giacomo Cavalli, and Thomas Cremer. Dy-  
473 namic genome architecture in the nuclear space: regulation of gene expression in three dimensions.  
474 *Nature Reviews Genetics*, 8(2):104–115, 2007.
- 475 [2] Boyan Bonev and Giacomo Cavalli. Organization and function of the 3D genome. *Nature Reviews  
476 Genetics*, 17(11):661–678, 2016.
- 477 [3] Thomas Cremer and Christoph Cremer. Chromosome territories, nuclear architecture and gene  
478 regulation in mammalian cells. *Nature Reviews Genetics*, 2(4):292, 2001.
- 479 [4] Bas van Steensel and Andrew S Belmont. Lamina-associated domains: Links with chromosome  
480 architecture, heterochromatin, and gene repression. *Cell*, 169(5):780–791, 2017.
- 481 [5] Erez Lieberman-Aiden, Nynke L Van Berkum, Louise Williams, Maxim Imakaev, Tobias Ragoczy,  
482 Agnes Telling, Ido Amit, Bryan R Lajoie, Peter J Sabo, Michael O Dorschner, et al. Comprehensive  
483 mapping of long-range interactions reveals folding principles of the human genome. *Science*, 326  
484 (5950):289–293, 2009.
- 485 [6] Suhas SP Rao, Miriam H Huntley, Neva C Durand, Elena K Stamenova, Ivan D Bochkov, James T  
486 Robinson, Adrian L Sanborn, Ido Machol, Arina D Omer, Eric S Lander, et al. A 3D map of  
487 the human genome at kilobase resolution reveals principles of chromatin looping. *Cell*, 159(7):  
488 1665–1680, 2014.
- 489 [7] Zhonghui Tang, Oscar Junhong Luo, Xingwang Li, Meizhen Zheng, Jacqueline Jufen Zhu, Prze-  
490 mysław Szalaj, Paweł Trzaskoma, Adriana Magalska, Jakub Włodarczyk, Blazej Ruszczycki, et al.  
491 CTCF-mediated human 3D genome architecture reveals chromatin topology for transcription. *Cell*,  
492 163(7):1611–1627, 2015.
- 493 [8] Jesse R Dixon, Siddarth Selvaraj, Feng Yue, Audrey Kim, Yan Li, Yin Shen, Ming Hu, Jun S Liu,  
494 and Bing Ren. Topological domains in mammalian genomes identified by analysis of chromatin  
495 interactions. *Nature*, 485(7398):376–380, 2012.
- 496 [9] Elphège P Nora, Bryan R Lajoie, Edda G Schulz, Luca Giorgetti, Ikuhiro Okamoto, Nicolas Ser-  
497 vant, Tristan Piolot, Nynke L van Berkum, Johannes Meisig, John Sedat, et al. Spatial partitioning  
498 of the regulatory landscape of the X-inactivation centre. *Nature*, 485(7398):381, 2012.
- 499 [10] Tom Misteli. Beyond the sequence: cellular organization of genome function. *Cell*, 128(4):787–  
500 800, 2007.
- 501 [11] Lars Guelen, Ludo Pagie, Emilie Brasset, Wouter Meuleman, Marius B Faza, Wendy Talhout,  
502 Bert H Eussen, Annelies de Klein, Lodewyk Wessels, Wouter de Laat, et al. Domain organization  
503 of human chromosomes revealed by mapping of nuclear lamina interactions. *Nature*, 453(7197):  
504 948, 2008.
- 505 [12] Yu Chen, Yang Zhang, Yuchuan Wang, Liguo Zhang, Eva K Brinkman, Stephen A Adam, Robert  
506 Goldman, Bas Van Steensel, Jian Ma, and Andrew S Belmont. Mapping 3D genome organization  
507 relative to nuclear compartments using TSA-Seq as a cytological ruler. *J Cell Biol*, 217(11):4025–  
508 4048, 2018.
- 509 [13] Mark B Gerstein, Anshul Kundaje, Manoj Hariharan, Stephen G Landt, Koon-Kiu Yan, Chao  
510 Cheng, Xinmeng Jasmine Mu, Ekta Khurana, Joel Rozowsky, Roger Alexander, et al. Architecture  
511 of the human regulatory network derived from ENCODE data. *Nature*, 489(7414):91–100, 2012.

- 512 [14] Daniel Marbach, David Lamparter, Gerald Quon, Manolis Kellis, Zoltán Kutalik, and Sven  
513 Bergmann. Tissue-specific regulatory circuits reveal variable modular perturbations across com-  
514 plex diseases. *Nature Methods*, 2016.
- 515 [15] Eric H Davidson. *The regulatory genome: gene regulatory networks in development and evolution*.  
516 Academic Press, San Diego, 2006.
- 517 [16] Samuel A Lambert, Arttu Jolma, Laura F Campitelli, Pratyush K Das, Yimeng Yin, Mihai Albu, Xi-  
518 aoting Chen, Jussi Taipale, Timothy R Hughes, and Matthew T Weirauch. The human transcription  
519 factors. *Cell*, 172(4):650–665, 2018.
- 520 [17] Stephanie Fanucchi, Youtaro Shibayama, Shaun Burd, Marc S Weinberg, and Musa M Mhlanga.  
521 Chromosomal contact permits transcription between coregulated genes. *Cell*, 155(3):606–620,  
522 2013.
- 523 [18] Steven T Kosak, David Scalzo, Sam V Alworth, Fusheng Li, Stephanie Palmer, Tariq Enver,  
524 James SJ Lee, and Mark Groudine. Coordinate gene regulation during hematopoiesis is related  
525 to genomic organization. *PLoS Biology*, 5(11):e309, 2007.
- 526 [19] Daniel S Neems, Arturo G Garza-Gongora, Erica D Smith, and Steven T Kosak. Topologically as-  
527 sociated domains enriched for lineage-specific genes reveal expression-dependent nuclear topolo-  
528 gies during myogenesis. *Proceedings of the National Academy of Sciences*, page 201521826, 2016.
- 529 [20] Indika Rajapakse, David Scalzo, Stephen J Tapscott, Steven T Kosak, and Mark Groudine. Net-  
530 working the nucleus. *Molecular Systems Biology*, 6(1):395, 2010.
- 531 [21] Haiming Chen, Jie Chen, Lindsey A Muir, Scott Ronquist, Walter Meixner, Mats Ljungman,  
532 Thomas Ried, Stephen Smale, and Indika Rajapakse. Functional organization of the human 4D  
533 nucleome. *Proceedings of the National Academy of Sciences*, 112(26):8002–8007, 2015.
- 534 [22] Xiaoyan Ma, Daphne Ezer, Boris Adryan, and Tim J Stevens. Canonical and single-cell Hi-C reveal  
535 distinct chromatin interaction sub-networks of mammalian transcription factors. *Genome Biology*,  
536 19(174), 2018.
- 537 [23] Ruggero Cortini and Guillaume J Filion. Theoretical principles of transcription factor traffic on  
538 folded chromatin. *Nature Communications*, 9, 2018.
- 539 [24] Austin R Benson, David F Gleich, and Jure Leskovec. Higher-order organization of complex net-  
540 works. *Science*, 353(6295):163–166, 2016.
- 541 [25] ENCODE Project Consortium et al. An integrated encyclopedia of DNA elements in the human  
542 genome. *Nature*, 489(7414):57, 2012.
- 543 [26] Tim Wang, Kivanç Birsoy, Nicholas W Hughes, Kevin M Krupczak, Yorick Post, Jenny J Wei,  
544 Eric S Lander, and David M Sabatini. Identification and characterization of essential genes in the  
545 human genome. *Science*, 350(6264):1096–1101, 2015.
- 546 [27] Marilyn Safran, Irina Dalah, Justin Alexander, Naomi Rosen, Tsippi Iny Stein, Michael Shmoish,  
547 Noam Nativ, Iris Bahir, Tirza Doniger, Hagit Krug, et al. GeneCards Version 3: the human gene  
548 integrator. *Database*, 2010, 2010.
- 549 [28] Sofia A Quinodoz, Noah Ollikainen, Barbara Tabak, Ali Palla, Jan Marten Schmidt, Elizabeth  
550 Detmar, Mason M Lai, Alexander A Shishkin, Prashant Bhat, Yodai Takei, et al. Higher-order  
551 inter-chromosomal hubs shape 3D genome organization in the nucleus. *Cell*, 2018.
- 552 [29] Attila Németh, Ana Conesa, Javier Santoyo-Lopez, Ignacio Medina, David Montaner, Bálint

- 553 Péterfia, Irina Solovei, Thomas Cremer, Joaquin Dopazo, and Gernot Längst. Initial genomics  
554 of the human nucleolus. *PLoS Genetics*, 6(3):e1000889, 2010.
- 555 [30] Peter J Thul, Lovisa Åkesson, Mikaela Wiking, Diana Mahdessian, Aikaterini Geladaki, Ham-  
556 mou Ait Blal, Tove Alm, Anna Asplund, Lars Björk, Lisa M Breckels, et al. A subcellular map of  
557 the human proteome. *Science*, 356(6340):eaal3321, 2017.
- 558 [31] Benjamin D Pope, Tyrone Ryba, Vishnu Dileep, Feng Yue, Weisheng Wu, Olgert Denas, Daniel L  
559 Vera, Yanli Wang, R Scott Hansen, Theresa K Canfield, et al. Topologically associating domains  
560 are stable units of replication-timing regulation. *Nature*, 515(7527):402, 2014.
- 561 [32] Denes Hnisz, Brian J Abraham, Tong Ihn Lee, Ashley Lau, Violaine Saint-André, Alla A Sigova,  
562 Heather A Hoke, and Richard A Young. Super-enhancers in the control of cell identity and disease.  
563 *Cell*, 155(4):934–947, 2013.
- 564 [33] Da Wei Huang, Brad T Sherman, and Richard A Lempicki. Bioinformatics enrichment tools: paths  
565 toward the comprehensive functional analysis of large gene lists. *Nucleic Acids Research*, 37(1):  
566 1–13, 2008.
- 567 [34] Eli Eisenberg and Erez Y Levanon. Human housekeeping genes, revisited. *Trends in Genetics*, 29  
568 (10):569–574, 2013.
- 569 [35] Jason Ernst and Manolis Kellis. Chromhmm: automating chromatin-state discovery and character-  
570 ization. *Nature Methods*, 9(3):215, 2012.
- 571 [36] Tri C Nguyen, Kathia Zaleta-Rivera, Xuerui Huang, Xiaofeng Dai, and Sheng Zhong. Rna, action  
572 through interactions. *Trends in Genetics*, 2018.
- 573 [37] David L Spector and Angus I Lamond. Nuclear speckles. *Cold Spring Harbor Perspectives in  
574 Biology*, 3(2):a000646, 2011.
- 575 [38] Yongdae Shin and Clifford P Brangwynne. Liquid phase condensation in cell physiology and  
576 disease. *Science*, 357(6357), September 2017.
- 577 [39] Denes Hnisz, Krishna Srinivas, Richard A Young, Arup K Chakraborty, and Phillip A Sharp. A  
578 phase separation model for transcriptional control. *Cell*, 169(1):13–23, March 2017.
- 579 [40] Ann Boija, Isaac A Klein, Benjamin R Sabari, Alessandra DallAgnese, Eliot L Coffey, Alicia V  
580 Zamudio, Charles H Li, Krishna Srinivas, John C Manteiga, Nancy M Hannett, et al. Transcription  
581 factors activate genes through the phase-separation capacity of their activation domains. *Cell*, 175  
582 (7):1842–1855, 2018.
- 583 [41] Fan Chung. Four Cheeger-type inequalities for graph partitioning algorithms. *Proceedings of  
584 ICCM, II*, pages 751–772, 2007.
- 585 [42] Charalampos E Tsourakakis, Jakub Pachocki, and Michael Mitzenmacher. Scalable motif-aware  
586 graph clustering. In *Proceedings of the 26th International Conference on World Wide Web*, pages  
587 1451–1460. International World Wide Web Conferences Steering Committee, 2017.
- 588 [43] Pan Li and Olgica Milenkovic. Inhomogeneous hypergraph clustering with applications. In *Ad-  
589 vances in Neural Information Processing Systems*, pages 2308–2318, 2017.
- 590 [44] Mikko Kivelä, Alex Arenas, Marc Barthelemy, James P Gleeson, Yamir Moreno, and Mason A  
591 Porter. Multilayer networks. *Journal of Complex Networks*, 2(3):203–271, 2014.
- 592 [45] Jonathan A Kelner, Lorenzo Orecchia, Aaron Sidford, and Zeyuan Allen Zhu. A simple, combi-  
593 natorial algorithm for solving sdd systems in nearly-linear time. In *Proceedings of the forty-fifth*

- 594 annual ACM symposium on Theory of computing, pages 911–920. ACM, 2013.
- 595 [46] R Scott Hansen, Sean Thomas, Richard Sandstrom, Theresa K Canfield, Robert E Thurman, Molly  
596 Weaver, Michael O Dorschner, Stanley M Gartler, and John A Stamatoyannopoulos. Sequencing  
597 newly replicated DNA reveals widespread plasticity in human replication timing. *Proceedings of  
598 the National Academy of Sciences*, 107(1):139–144, 2010.
- 599 [47] Robert E Thurman, Nathan Day, William S Noble, and John A Stamatoyannopoulos. Identification  
600 of higher-order functional domains in the human ENCODE regions. *Genome Research*, 17(6):  
601 917–927, 2007.
- 602 [48] Kate R Rosenbloom, Cricket A Sloan, Venkat S Malladi, Timothy R Dreszer, Katrina Learned,  
603 Vanessa M Kirkup, Matthew C Wong, Morgan Maddren, Ruihua Fang, Steven G Heitner, et al.  
604 ENCODE data in the UCSC Genome Browser: year 5 update. *Nucleic Acids Research*, 41(D1):  
605 D56–D63, 2012.
- 606 [49] Edward L Huttlin, Raphael J Bruckner, Joao A Paulo, Joe R Cannon, Lily Ting, Kurt Baltier, Greg  
607 Colby, Fana Gebreab, Melanie P Gygi, Hannah Parzen, et al. Architecture of the human interactome  
608 defines protein communities and disease networks. *Nature*, 2017.
- 609 [50] Andrew Chatr-Aryamontri, Bobby-Joe Breitkreutz, Sven Heinicke, Lorrie Boucher, Andrew Win-  
610 ter, Chris Stark, Julie Nixon, Lindsay Ramage, Nadine Kolas, Lara O'Donnell, et al. The BioGRID  
611 interaction database: 2013 update. *Nucleic Acids Research*, 41(D1):D816–D823, 2012.
- 612 [51] Andreas Ruepp, Brigitte Waegele, Martin Lechner, Barbara Brauner, Irmtraud Dunger-Kaltenbach,  
613 Gisela Fobo, Goar Frishman, Corinna Montrone, and H-Werner Mewes. CORUM: the compre-  
614 hensive resource of mammalian protein complexes-2009. *Nucleic Acids Research*, 38(suppl\_1):  
615 D497–D501, 2009.
- 616 [52] Andrea Franceschini, Damian Szklarczyk, Sune Frankild, Michael Kuhn, Milan Simonovic,  
617 Alexander Roth, Jianyi Lin, Pablo Minguez, Peer Bork, Christian Von Mering, et al. STRING  
618 v9. 1: protein-protein interaction networks, with increased coverage and integration. *Nucleic Acids  
619 Research*, 41(D1):D808–D815, 2012.

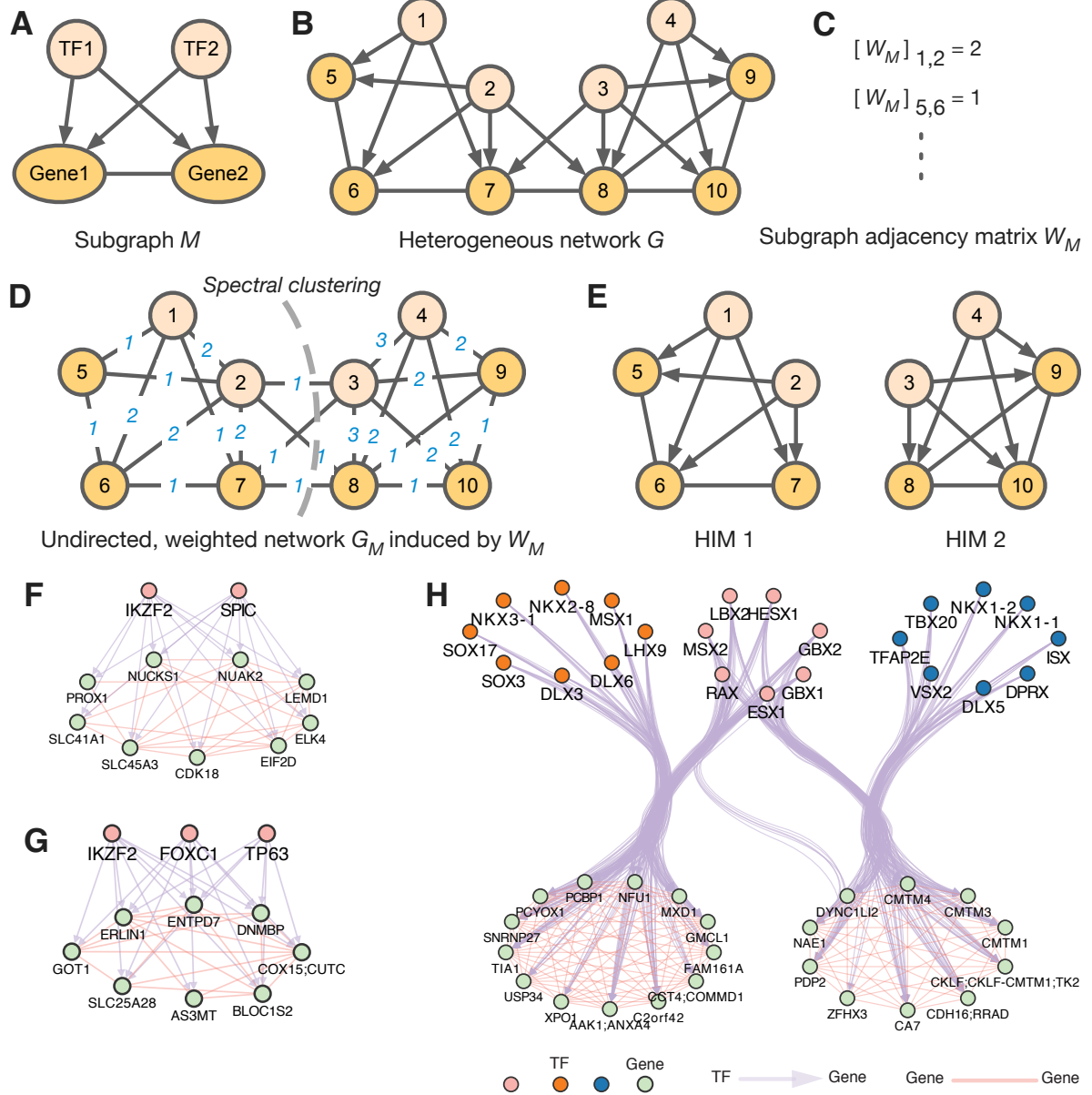


**Figure 1:** Workflow of our MOCHI algorithm and output examples of HIMs. The network has both gene-gene spatial proximity and TF-gene regulation relationships. **(A)** A 4-node motif  $M$  represents the smallest HIM. Here directed interaction represents a TF-gene regulation relationship, an undirected interaction represents that the two genes are spatially more proximal to each other than expected. **(B)** Given a heterogeneous network  $G$ , we find HIMs by minimizing the motif conductance (see Eq. 2). **(C)** We compute the subgraph adjacency matrix  $W_M$  with  $[W_M]_{ij}$  being the number of occurrences of  $M$  that have both nodes  $i$  and  $j$ . **(D)** The weighted network  $G_M$  is defined from adjacency matrix  $W_M$ . **(E)** Spectral clustering will find clusters in  $G_M$ . We recursively apply the method to find multiple HIMs and overlapping HIMs. **(F-G)** Two HIMs as examples in GM12878. **(H)** Example of two overlapping HIMs in GM12878 sharing 7 TFs (the group with pink nodes). TFs in orange and pink nodes form one HIM with their target genes (bottom left). TFs in pink and blue nodes form another HIM with their target genes (bottom right). Note that the directed interactions from TFs to their target genes are bundled.

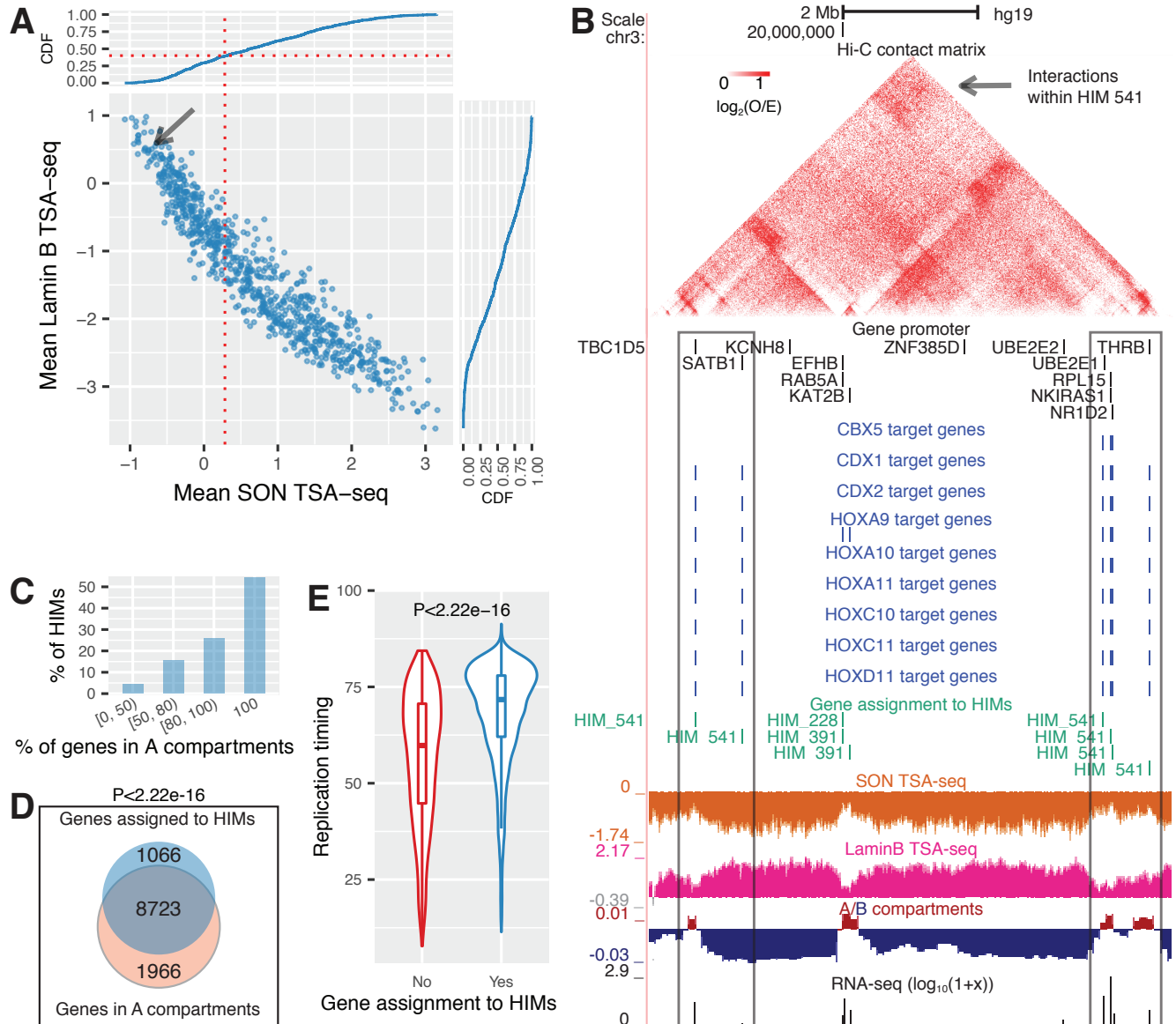


**Figure 2:** HIMs tend to be close to nuclear interior, in particular, speckles. **(A)** Scatter plot shows the mean SON TSA-seq score and mean Lamin B TSA-seq score of the genes in each HIM. Each dot represents a HIM. The curves on top and right are cumulative density functions (CDF). The red vertical dotted line represents the mean SON TSA-seq at 0.284 (approx. within 0.518 μm of nuclear speckles [12]). The black arrow points to HIM #541. **(B)** HIM #541 with low mean SON TSA-seq (pointed by the arrow in **(A)**). The heatmap shows the upper-triangle part of the Hi-C contact matrix (O/E) of the 10kb-sized bins in the chromosome region that covers the genes in the HIM. Target genes of different TFs, gene members of HIM, SON TSA-seq, LaminB TSA-seq, A/B compartments, and RNA-seq signals are shown in different tracks. **(C)** Barplot shows the proportion of HIMs with a varied proportion of genes in A compartment. **(D)** Venn diagram shows that the genes assigned to HIMs are enriched in A compartment. **(E)** Violin and boxplot compare the replication timing of the genes assigned to HIMs and the other genes in the heterogeneous network of K562. Here the HIMs are identified in K562 cell line. The spatial location features of HIMs in other cell types are in Fig. S2.

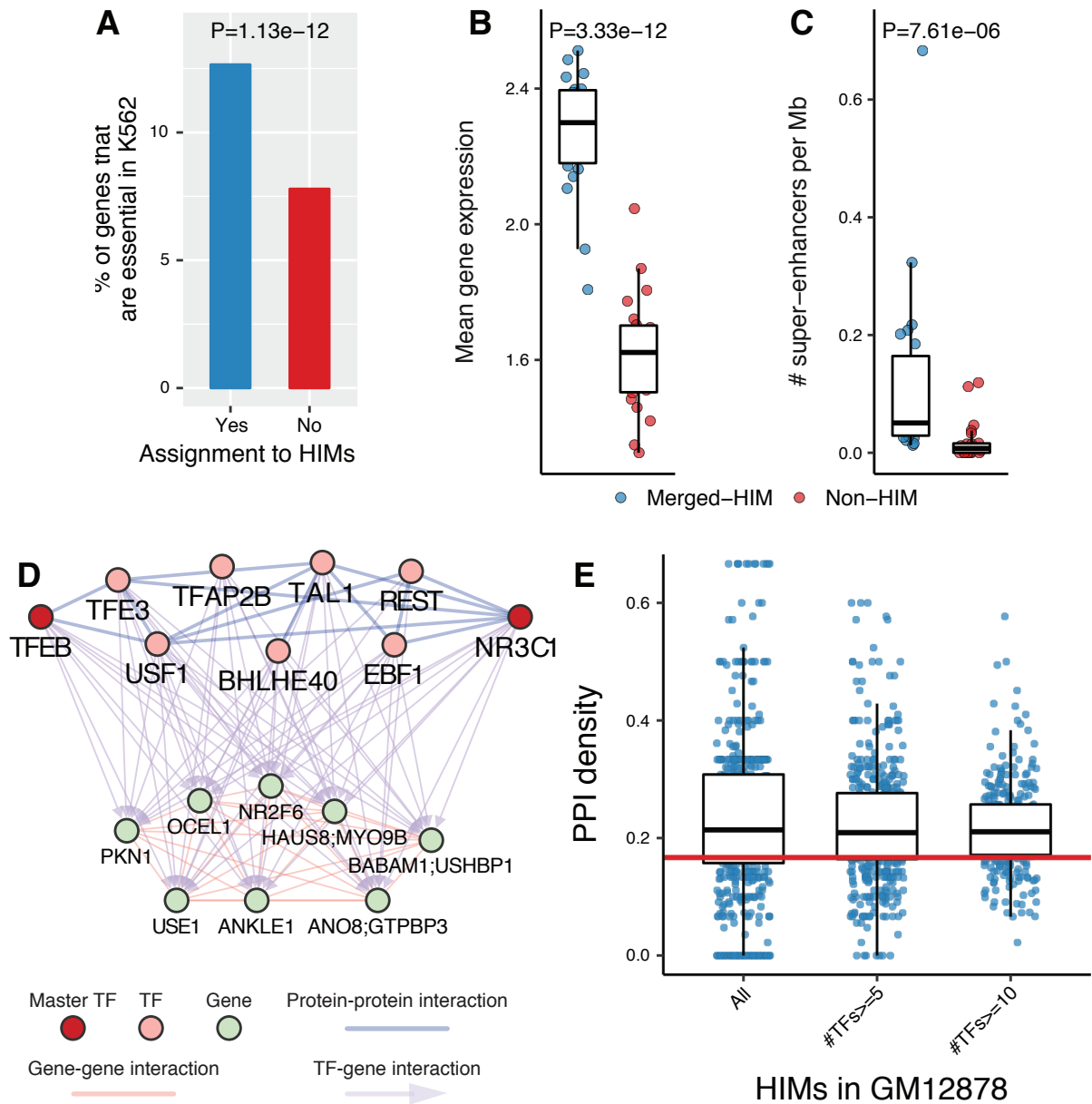


**Figure 3:** HIMs are enriched with essential genes, super-enhancers, and protein-protein interactions. **(A)** Barplots show the proportions of genes that are K562 essential genes among the genes assigned to HIMs and those not assigned to HIMs. **(B-C)** Functional properties of the genes in the identified HIMs in K562. To make a fair comparison, we stratified the genes assigned to HIMs by chromosome number and called resulted clusters as merged-HIM clusters. Similarly, we derived non-HIM clusters from the genes in the heterogeneous networks but not assigned to HIMs. P-values are computed by the paired two-sample Wilcoxon rank-sum test. **(B)** Boxplot shows the average gene expression level of the genes in a cluster. **(C)** Boxplot shows the normalized number of super-enhancers related to a cluster. **(D-E)** TFs in HIMs are enriched with protein-protein interactions (PPIs) among themselves. **(D)** One example of HIM from GM12878 cell line shows that 9 TFs in the HIM are connected by 14 PPI interactions. The sub-PPI network has a density at 0.389. The TFs NR3C1 and TFE3 are master TFs in GM12878. **(E)** Boxplots show the distribution of the sub-PPI network density of the HIMs and the subsets of HIMs with at least  $n$  TFs,  $n = 5, 10$ . The medians are significantly ( $p < 2.22 \times 10^{-16}$ ) higher than the expected density (0.158, red line) of the sub-PPI networks induced by randomly sampled TFs.

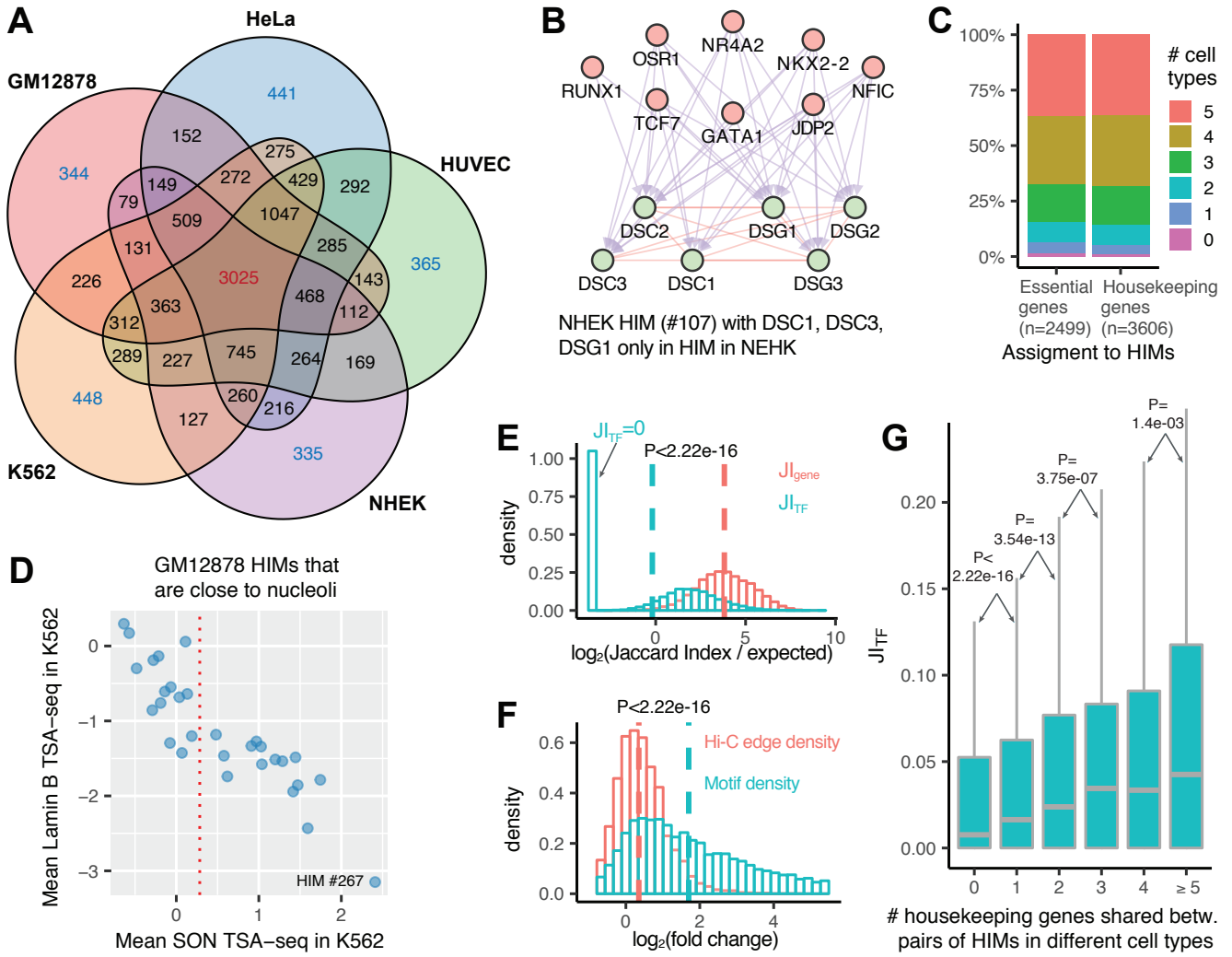


**Figure 4:** HM comparisons in terms of genes and TFs across the cell types. **(A)** Venn diagram shows the assignment of genes in HMs across five cell type. Numbers in each facet represent the gene number in each possible logic intersection relationship across five cell types. **(B)** A NHEK HM with 3 genes only assigned to HMs in NHEK. All of its genes are involved in keratinization pathway. Here the top and bottom nodes are the TFs and genes in the HM, respectively. **(C)** Barplot shows the assignment of essential genes and housekeeping genes to HMs across five cell types. **(D)** Scatter plot shows the mean SON TSA-seq and Lamin B TSA-seq scores (in K562 [12]) of the 30 GM12878 HMs that are inferred as close to nucleoli in GM12878 [28]. The red vertical dotted line represents the mean SON TSA-seq score at 0.284. **(E)** The log-transformed ratio of Jaccard index on the genes/TFs between paired HMs from different cell types over the expected Jaccard index between random control sets. **(F)** Fold changes of motif *M* density and Hi-C edge density of each HM between the cell type it is identified and another cell type. Here a vertical dash line represents the median of a variable. **(G)** Boxplots show the distribution of Jaccard index on the TFs of paired HMs with different numbers of shared housekeeping genes.

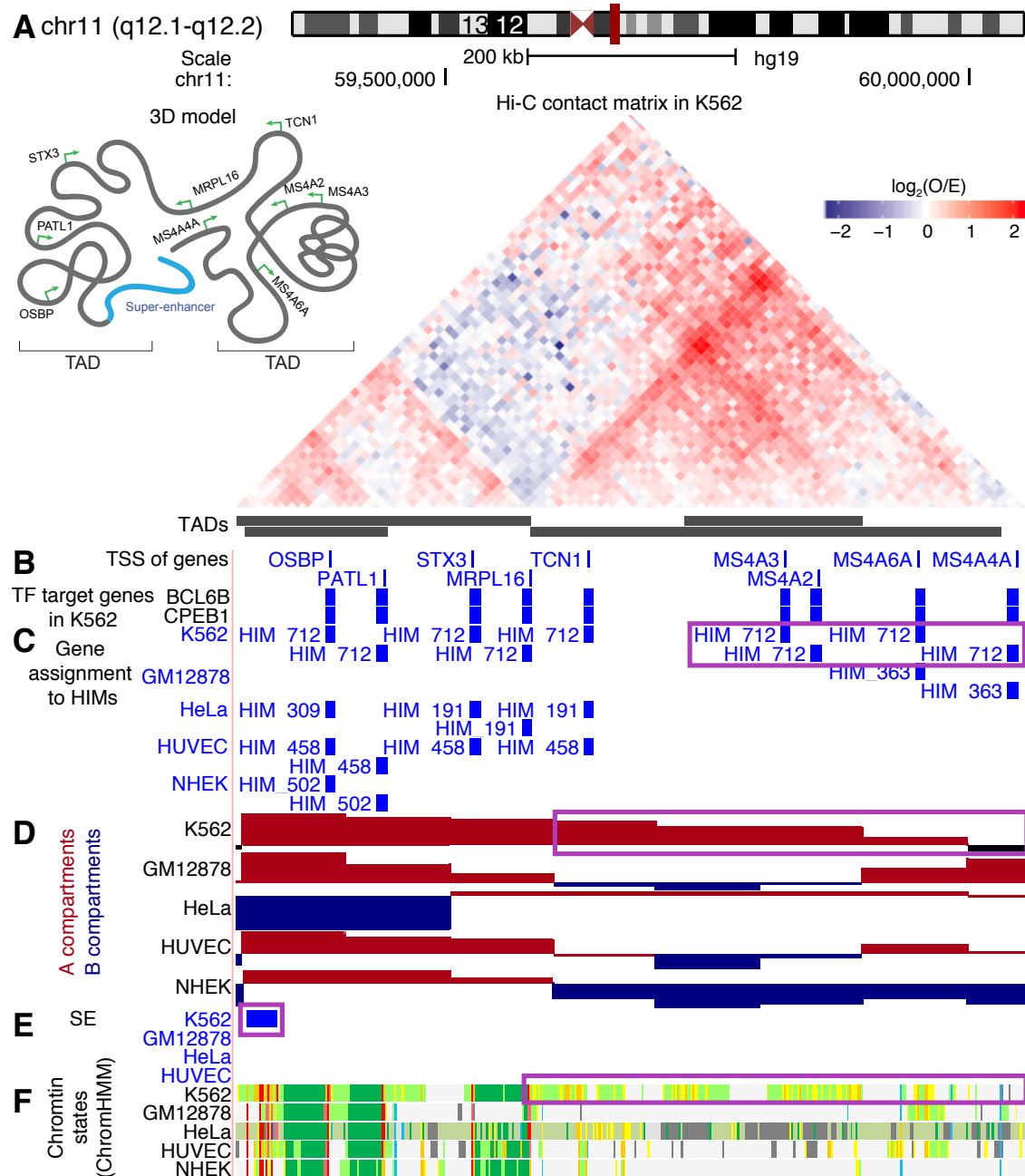


**Figure 5:** A K562 specific HIM with K562 specific chromatin interactome and functional annotations. **(A)** The 45 degree rotated upper triangle part of the contact matrix between the 10kb-sized bins in a chromosome region in K562. The region is segregated into 4 nested TADs. **(B)** Thin bars represent the transcriptional start sites (TSSs) of the genes that are in the heterogeneous networks. Thick bars represent the genes that are regulated by BCL6B or CPEB1 in K562. **(C)** The assignment of the genes to HIMs in K562 and the other cell types. **(D)** The assignment of the bins to A/B compartments. **(E)** The regions that are annotated as super-enhancers (SE). **(F)** The chromatin states inferred by ChromHMM based on multiple histone modification marks, where red and purple colors represent promoters, orange and yellow stand for enhancers, green represents transcribed regions, gray represents other types of regions such as repressed regions.

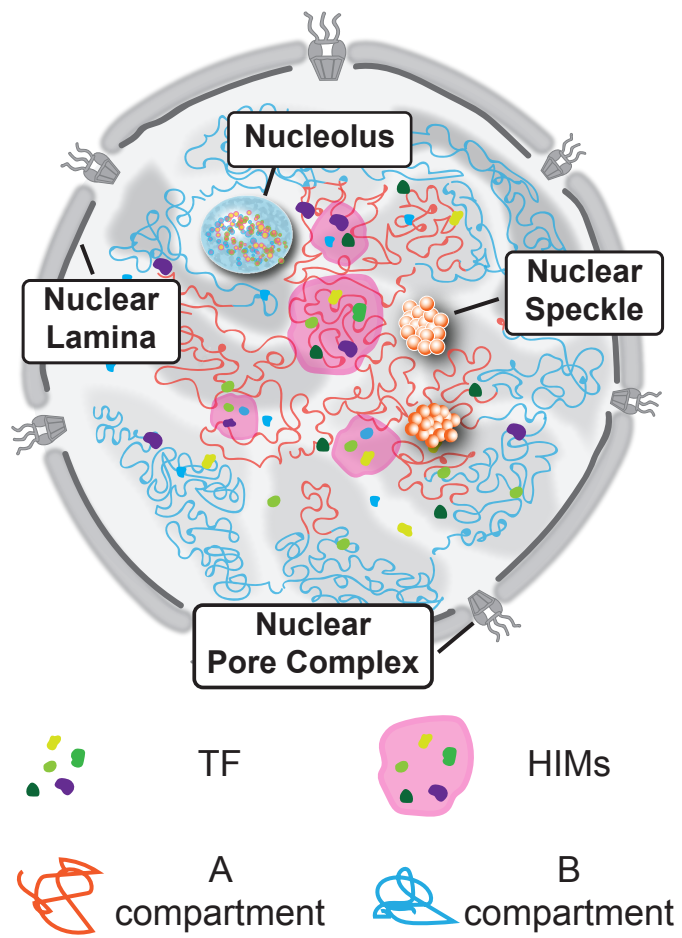


**Figure 6:** A possible model of HIMs within the nucleus.

620 **Supplemental Information**

621 **A Supplementary Methods**

622 **A.1 Pseudocode for the MOCHI algorithm**

---

**Algorithm 1** MOCHI

**Require:** Original graph  $G_0$ , motif  $M$ , threshold  $t_1$ .

**Ensure:** Network motif based clusters

```
1: function ITERATIVE SPECTRAL CLUSTERING( $G_0, M, t_1$ )
2:    $W_M(G_0) \leftarrow$  Motif adjacency matrix for  $G_0$  based on motif  $M$ 
3:    $S_0, \bar{S}_0, Score_0 =$  SPECTRAL CLUSTERING( $W_M(G_0), N$ )
4:    $L \leftarrow \{G_0\}$ 
5:
6:   while  $\exists G_i \in L$  such that  $Score_i < t_1$ , do
7:      $G_k \leftarrow \text{argmin}_i Score_i$  The graph with the lowest corresponding score
8:      $G_{S_k}, G_{\bar{S}_k} \leftarrow$  Graph for node set  $S_k, \bar{S}_k$ , respectively
9:      $W_M(G_{S_k}), W_M(G_{\bar{S}_k}) \leftarrow$  Motif adjacency matrix for  $G_{S_k}, G_{\bar{S}_k}$ 
10:    Drop all-zero rows and columns in  $W_M(G_{S_k}), W_M(G_{\bar{S}_k})$  and corresponding nodes in
        $G_{S_k}, G_{\bar{S}_k}$ 
11:     $N_{S_k}, N_{\bar{S}_k} \leftarrow$  Node size of  $G_{S_k}, G_{\bar{S}_k}$ , respectively
12:     $S_{S_k}, \bar{S}_{S_k}, Score_{S_k} =$  SPECTRAL CLUSTERING( $W_M(G_{S_k}), N_{S_k}$ )
13:     $S_{\bar{S}_k}, \bar{S}_{\bar{S}_k}, Score_{\bar{S}_k} =$  SPECTRAL CLUSTERING( $W_M(G_{\bar{S}_k}), N_{\bar{S}_k}$ )
14:     $L \leftarrow \{..., G_{k-1}, G_{k+1}, ..., G_{S_k}, G_{\bar{S}_k}\}$ 
15:  end while
16: end function
17:
18: function SPECTRAL CLUSTERING( $W_M, N$ )
19:    $D \leftarrow$  Diagonal Matrix(1:N × 1:N) given by  $D_{ii} = \sum_{j=1}^N (W_M)_{ij}$ 
20:    $L \leftarrow D^{-\frac{1}{2}}(D - W_M)D^{-\frac{1}{2}}$ 
21:    $v = \{v_1, v_2, ..., v_N\} \leftarrow$  Eigenvector of  $L$ 
22:    $v_k \in v \leftarrow$  Eigenvector of the second smallest eigenvalue
23:    $O \leftarrow D^{-\frac{1}{2}}v_k$ 
24:    $\alpha_i \leftarrow$  Index of the  $i$ -th smallest value in  $O$ 
25:    $S \leftarrow \text{argmin}_k \varphi_{G_M}(S_k)$ , where  $S_k = \{\alpha_1, \dots, \alpha_k\}$ 
26:    $Score \leftarrow \varphi_{G_M}(S)$ 
27:   return  $S, \bar{S}, Score$ 
28: end function
```

---

623 **A.2 Computational complexity**

624 Here we analyze the computational complexity of MOCHI. In practice, the most time-consuming step
625 would be the construction of the motif adjacency matrix  $W_M$  and the calculation of the eigenvector for

the normalized Laplacian matrix. Although in general for eigenvalue decomposition of a matrix size of  $N \times N$ , the runtime would be  $O(N^3)$ , using fast symmetric diagonally dominant solvers for Laplacian matrix, we can reach near linear time for this process [45]. Therefore, in the rest of this section, we will only discuss the computational complexity of the matrix construction part.

Intuitively, for a 4-node motif, we can calculate  $W_M$  by checking every combination of 4 nodes in the graph, and has the complexity of  $O(N^4)$ , where  $N$  is the number of nodes in the graph. However, here since we only deal with a special 4-node motif that consists of 2 different types of nodes, which can be treated as a combination of two specific 3-node motifs (one TF regulates two genes), if we use  $T$  for the TF nodes in the graph, and  $C$  for the chromatin loci nodes, and  $t, c$  for the size of these nodes, respectively, we can derive the runtime as follows. For  $W_{M_{ij}}$  in the motif adjacency matrix, where  $i \in C, j \in C$ , it is equivalent to finding the number  $n_{3ij}$  of specific 3-node motif that  $i$  and  $j$  share, then using the combination number to get the number of 4-node motif  $n_{4ij} = \binom{n_{3ij}}{2}$ . For the search of triangles, given  $i$  and its neighbor  $j$ , we sum up all the TF nodes that they share, which gives us the complexity of  $O(tc^2)$ . For  $W_{M_{ij}}$ , where  $i \in T, j \in C$ , as we already know how many 3-node motifs would form between locus  $j$  and any another locus  $k$  (as calculated above), we can also calculate the number of 4-node motifs involving  $i, j$  by counting the 3-node motifs using the similar method. The complexity of this part would also be  $O(tc^2)$ . Finally, for the  $W_{M_{ij}}$ , where  $i \in T, j \in T$ , we cannot count the 3-node triangle anymore. To count the number of 4-node motifs involving  $i, j$ , we find out the common loci they share, and then calculate the total number of edges between these common loci. To summarize, the runtime for the whole algorithm is dominated by the construction of  $W_M$ , especially for the part between TF and TF. The worst case runtime would be  $O(t^2c^2)$ , where we have to go over all the combination of two TF and two gene loci. Note that, however, TFs only make up a small part of the nodes (about 4.5%). Also, as the network is somehow sparse, usually, we do not need to go over all the combination of nodes, which would accelerate the computation further. In addition, in the actual implementation, we use parallel computation to further speed up the process, which makes the entire algorithm quite efficient in practice.

### A.3 Clusters are near optimal

Here we prove that the two clusters from Steps (1) and (2) described in the algorithm in the main text are near optimal when  $\alpha = 4/3$  in Eq. (3). Without loss of generality, we prove that the two clusters  $S$  and  $\bar{S}$  of the original heterogeneous network  $G$  are near optimal. By definition,  $\varphi_M(S) = \varphi_M(\bar{S})$ , thus we only need to show that  $S$  is near optimal.

We first formally state the near optimal claim and prove it in the subsequent paragraphs. Let  $\varphi_M^*$  be the minimum of subgraph conductance over all possible sets of nodes in  $G$ . Then  $S$  satisfies motif Cheeger inequality [41], i.e.,

$$\varphi_M(S) \leq 4\sqrt{\varphi_M^*} \leq 1 \quad (7)$$

which means that  $S$  is at most a quadratic factor away from the optimal cluster that achieves  $\varphi_M^*$ .

We recall and define some mathematical notations. Let  $N$  be the total number of nodes in  $G$ . Let  $M$  be the subgraph with four nodes and five interactions, where the four nodes are 2 TFs and 2 genes. Four of the five interactions are interactions between TFs and genes. The fifth interaction is between the two genes. Let  $V_M$  be the set of the four nodes of  $M$ . Let  $|V_M|$  denote the cardinality of  $V_M$ . Here  $|V_M| = 4$ . Let  $\mathbb{M}$  be the set of the occurrences of  $M$  in  $G$ . Let  $W_M$  denote the subgraph adjacency matrix where

<sup>666</sup>  $[W_M]_{ij} = \sum_{M \in \mathbb{M}} \mathbb{1}(i \in V_M, j \in V_M)$ . The undirected weighted network induced by  $W_M$  is denoted  
<sup>667</sup> by  $G_M$ . The subgraph conductance  $\varphi_M(S)$  for  $G$  is defined in Eq. (8) and the conductance  $\varphi_{G_M}(S)$  is  
<sup>668</sup> defined in Eq. (9):

$$\varphi_M(S) = \frac{\text{cut}_M(S, \bar{S})}{\min[\text{Vol}_M(S), \text{Vol}_M(\bar{S})]} \quad (8)$$

$$\varphi_{G_M}(S) = \frac{\text{cut}_{G_M}(S, \bar{S})}{\min[\text{Vol}_{G_M}(S), \text{Vol}_{G_M}(\bar{S})]} \quad (9)$$

<sup>669</sup> First, we prove that  $\text{cut}_M(S, \bar{S}) = \frac{1}{3}\text{cut}_{G_M}(S, \bar{S})$ . Let  $X = (x_1, x_2, \dots, x_N)$  be the vector denoting  
<sup>670</sup> which nodes belong to  $S$ . If node  $i$  belongs to  $S$ , then  $x_i = -1$ . Otherwise,  $x_i = 1$ . Let  $v_1, v_2, v_3, v_4$  be  
<sup>671</sup> the four nodes in an occurrence of the subgraph  $M \in \mathbb{M}$ . We have:

$$\begin{aligned} \text{cut}_M(S, \bar{S}) &= \sum_{M \in \mathbb{M}} \mathbb{1}(|V_M \cap S| \in \{1, 3\}) + \frac{4}{3} \sum_{M \in \mathbb{M}} \mathbb{1}(|V_M \cap S| = 2) \\ &= \sum_{M \in \mathbb{M}} \frac{6 \mathbb{1}(|V_M \cap S| \in \{1, 3\}) + 8 \mathbb{1}(|V_M \cap S| = 2)}{6} \\ &= \sum_{M \in \mathbb{M}} \frac{6 - x_{v_1}x_{v_2} - x_{v_1}x_{v_3} - x_{v_1}x_{v_4} - x_{v_2}x_{v_3} - x_{v_2}x_{v_4} - x_{v_3}x_{v_4}}{6} \\ &= \sum_{M \in \mathbb{M}} \frac{\frac{3}{2}(x_{v_1}^2 + x_{v_2}^2 + x_{v_3}^2 + x_{v_4}^2) - (x_{v_1}x_{v_2} + x_{v_1}x_{v_3} + x_{v_1}x_{v_4} + x_{v_2}x_{v_3} + x_{v_2}x_{v_4} + x_{v_3}x_{v_4})}{6} \\ &= \frac{\frac{1}{2}x^T D_M x - \frac{1}{2}x^T W_M x}{6} \\ &= \frac{2 \times \text{cut}_{G_M}(S)}{6} \\ &= \frac{1}{3}\text{cut}_{G_M}(S). \end{aligned}$$

<sup>672</sup> Next, we show that  $\text{Vol}_M(S) = \frac{1}{3}\text{Vol}_{G_M}(S)$ . Note that  $|V_M| = 4$ .

$$\begin{aligned} \text{Vol}_M(S) &= \sum_{i \in S} \sum_{M \in \mathbb{M}} \mathbb{1}(i \in V_M) \\ &= \sum_{i \in S} \sum_{M \in \mathbb{M}} \frac{1}{3} \sum_{j \in V_M} \mathbb{1}(|\{i, j\} \cap V_M| = 2) \\ &= \sum_{i \in S} \sum_{M \in \mathbb{M}} \frac{1}{3} \sum_{j=1}^N \mathbb{1}(|\{i, j\} \cap V_M| = 2) \\ &= \frac{1}{3} \sum_{i \in S} \sum_{j=1}^N \sum_{M \in \mathbb{M}} \mathbb{1}(|\{i, j\} \cap V_M| = 2) \\ &= \frac{1}{3} \sum_{i \in S} \sum_{j=1}^N [W_M]_{ij} \\ &= \frac{1}{3}\text{Vol}_{G_M}(S). \end{aligned}$$

673 We have  $\varphi_M(S) = \varphi_{G_M}(S)$  by definitions in Eq. (8), Eq. (9), and that  $\text{cut}_M(S, \bar{S}) = \text{cut}_{G_M}(S)$  and  
674  $\text{Vol}_M(S) = \text{Vol}_{G_M}(S)$ .

675 Finally, let  $\varphi_{G_M}^*$  be the minimum of conductance over all possible sets of nodes  $G_M$ . Then  $S$  satisfies  
676 the Cheeger inequality, i.e.,

$$\varphi_{G_M}(S) \leq 4\sqrt{\varphi_{G_M}^*} \leq 1. \quad (10)$$

677 *Comparison with the proofs in Benson et al. [24]*

678 In Step (2), we apply a spectral clustering method to find two sets  $S$  and  $\bar{S}$  in the undirected, weighted  
679 network  $G_M$  that is induced by  $W_M$ . The spectral clustering method is the same as the method in [24]  
680 where  $W_M$  is computed based on a homogeneous motif and homogeneous network. Benson et al. [24]  
681 proved that  $S$  and  $\bar{S}$  are near optimal for their case. However, the results in [24] are not applicable to our  
682 situation, because our input network and motif are heterogeneous, and converting the heterogeneous net-  
683 work and motif to homogeneous network and motif will mis-count the occurrences of the heterogeneous  
684 motif  $M$ . However, our proofs follow the same strategy as the proofs in [24].

685 **A.4 Properties of the identified HIMs**

686 Here we describe the properties of HIMs that are not defined in the main text. The features are the  
687 topological structural features related to connection patterns of the genes and TFs in a given HIM within  
688 a heterogeneous network, including motif density, chromatin interaction edge density (or Hi-C edge  
689 density), and GRN edge density, which quantify the connection strength between genes/TFs in a HIM in  
690 terms of different connection patterns. All range from 0 to 1.

- 691 • 4-node motif  $M$  density. It is the ratio of the number of occurrences of the motif  $M$  to the total  
692 number of possible occurrences of the motif  $M$  in a HIM. The maximal motif density is 1, which  
693 is achieved when every pair of genes in the cluster are connected with Hi-C interactions and every  
694 gene is regulated by each TF in the cluster. The triangle motif density used later in Supplemental  
695 Information B.2 is defined similarly.
- 696 • Hi-C edge density. It is the density of the sub-Hi-C interaction network induced by the genes in  
697 the HIM. The Hi-C edge density at 1 means that every pair of genes is connected by a chromatin  
698 interaction with O/E>1, where 0 means that no pair of genes is connected. Thus a higher density  
699 means that the HIM genes as a unit are more densely packed in the nucleus.
- 700 • GRN edge density. It is the density of the sub-GRN induced by the genes and TFs in the HIM.  
701 The maximal 1 is achieved when every gene is regulated by every TF in the HIM. The minimal 0  
702 is achieved when TF-gene interaction does not exist in a HIM.

703 **A.5 Collection and processing of data used in this study**

704 In this work, we use data for five human cell types: GM12878, HeLa, HUVEC, K562, and NHEK.  
705 For Hi-C related data, including KR normalized contact frequency matrices by in-situ Hi-C and O/E  
706 contact frequency matrices were from [6]. We downloaded the data from GEO with the accession num-  
707 ber GSE63525. We calculated the A/B compartments for each chromosome using the first principal  
708 component of the O/E contact frequency matrix as the same in [5]. For intra-chromosomal contacts,  
709 we first filtered the genome-wide KR normalized contact matrix by only keeping intra-chromosomal  
710 contacts higher than expected values, aiming to reduce intra-chromosomal contacts due to random chro-  
711 matin collisions. In addition, we used the size of compartments to control the 1D distance between

712 genes farthest apart in HIMs. The 99-th percentile of the size of compartments is around 10Mb in  
713 4 out of the 5 cell types. Thus we chose the 1D distance cutoff universally as 10Mb and only kept  
714 the remaining intra-chromosome contacts that connect bins within 10Mb across the cell types. Then  
715 only the top 1% inter-chromosomal contacts were kept by choosing the cutoff as the 99-th percentile of  
716 the genome-wide inter-chromosomal contacts. The remaining inter-chromosomal contacts have at least  
717 2.17 KR normalized Hi-C contacts. Processed replication timing data with the GEO accession number  
718 GSE34399 [46, 47] were downloaded from the UCSC Genome Browser [48].

719 GRN data were downloaded from [14], where directed TF-gene interactions were inferred by simul-  
720 taneously considering the TF binding motifs and gene expression level. Briefly, an interaction between  
721 a TF and a gene is called if (1) the TF has enriched binding motifs on the enhancer or promoter regions  
722 of the gene; and (2) the co-expression level between the TF and the enhancer or promoter of the gene is  
723 high.

724 Protein-protein interactions (PPIs) were downloaded from BioPlex2 [49], BioGrid [50], CORUM [51],  
725 and STRING [52]. We first extracted the PPIs between the 591 TFs in the GRNs from these public  
726 sources. We then combined them into a PPI network after merging duplicated PPIs. Note that the GRNs  
727 have the same set of TF protein. Thus the PPI network is suitable for all 5 different cell types. The  
728 density of the PPI network is 0.158, which is also the expected density of a sub-PPI network of a set of  
729 randomly sampled TFs.

730 Essential genes in four cell lines were downloaded from [26]. However, among the four cell lines,  
731 only K562 matches the cell types used in this study. The essential genes identified in K562 were only  
732 used to analyze identified HIMs in K562. Because the majority of the essential genes are shared between  
733 the 4 cancer cell lines [26], we used the union of them as the essential gene list in GM12878, HeLa,  
734 HUVEC, and NHEK cell types. The union has 2741 essential genes.

735 RNA-seq data with GEO accession # GSE33480 were downloaded from the ENCODE project [25].  
736 The gene expression level quantified in FPKM value across the 5 cell types were normalized by quantile  
737 normalization then logarithm transformed by the function  $\log_{10}(1 + x)$ . From the expression data, we  
738 constructed a list of cell type-specific genes for each cell type by the following two criteria. Given a  
739 cell type, (1) the gene expression value in the given cell type is higher than 0.1; (2) the ratio of the gene  
740 expression value in the given cell type to the median gene expression value in the other 4 cell types is  
741 higher than 2.

742 **B Supplementary Results**

743 **B.1 HIMs are robust to the parameters used to construct the heterogeneous networks**

744 We show that the identified HIMs in the main text are robust to the parameters used to define the het-  
745 erogeneous networks. In all the analysis presented in the main text, we use a cutoff at 1 for “observed  
746 over expected” (O/E) quantity to filter out intra-chromosomal Hi-C contacts when defining chromatin  
747 interaction networks. To test the robustness of HIMs, we construct another set of chromatin interaction  
748 networks by the cutoff at 2 (for O/E). The number of intra-chromosomal chromatin interactions with the  
749 cutoff at 2 is 64.6%-81.9% of the number of intra-chromosomal interactions with the cutoff at 1 across  
750 five cell types. We denote the sub-Hi-C interaction networks resulted from the cutoff at 2 as sub-Hi-C.  
751 Regarding GRNs, we also construct a sub-GRN for each cell type by only keeping the top 90% interac-  
752 tions with the highest scores. We then construct 3 different heterogeneous networks for each cell type as  
753 follows:

- 754 • The heterogeneous network combines the chromatin interaction network with the cutoff at 1 and  
755 the whole GRN. This is the heterogeneous network used in the main text. The heterogeneous  
756 network is referred as Hi-C + GRN.
- 757 • The heterogeneous network combines the chromatin interaction network with the cutoff at 2 and  
758 the whole GRN. The heterogeneous network is referred as sub-Hi-C + GRN.
- 759 • The heterogeneous network combines the chromatin interaction network with the cutoff at 1 and  
760 the sub-GRN. The heterogeneous network is referred to as Hi-C + sub-GRN.

761 We apply MOCHI with the 4-node motif  $M$  to each of the 3 heterogeneous networks of each cell type.  
762 We use adjusted Rand index to quantify the similarities on gene memberships between the HIMs from  
763 two different heterogeneous networks. For example, if the assignment of genes to HIMs are identical  
764 between two sets of HIMs, then adjusted Rand index would be 1. We use hierarchical clustering to  
765 group the sets of HIMs with similar adjusted Rand index. We found that the sets of HIMs from the  
766 heterogeneous networks of the same cell type are much more similar to each other than to the sets of  
767 HIMs from the other cell types. Hierarchical clustering produces five major clusters (Fig. S10). Each  
768 cluster contains 3 different heterogeneous networks in the same cell type. Overall, the result suggests  
769 that the HIMs are less sensitive to the parameters used in constructing the chromatin interactome and  
770 GRNs.

771 **B.2 Justification of the 4-node motif  $M$**

772 To justify the choice of the motif  $M$ , we compared it with two different types of motifs. One is a triangle  
773 motif with 3 nodes (Fig. S11A), where two of them are genes with a chromatin interaction and the third  
774 node is a TF that regulates both the genes. The triangle motif does not explicitly encode co-regulation  
775 between TF proteins. Another motif is a bifan motif with 4 nodes (Fig. S11A), where two nodes are TF  
776 proteins that co-regulate two genes but there is no chromatin interaction between the two genes. The  
777 bifan motif does not explicitly encode spatial proximal relationship between genes. For bifan motif, we  
778 applied MOCHI with the bifan on the GRN and then split the identified HIMs by chromosome number.

779 We found that the motif  $M$  and triangle motif are better than the bifan motif in terms of identifying  
780 the clusters (Fig. S11B). Compared to the HIMs identified by the bifan motif, the HIMs by the motif  
781  $M$  and triangle motif have higher Hi-C edge density, higher triangle density, higher motif  $M$  density.

782 Moreover, the genes in a HIM are closer to each other in the 1D sequence space, although the HIMs by  
 783 the bifan motif have a smaller number of genes as compared to the HIMs by the motifs  $M$  and triangle.  
 784 This result highlights that the chromatin interaction between the two target genes in a motif is important  
 785 to capture spatial proximity between the genes in HIMs.

786 In addition, we found that our motif  $M$  is better than the triangle motif. We comprehensively com-  
 787 pared the identified HIMs by the motif  $M$  and the triangle motif. The HIMs identified by the two motifs  
 788 have similar numbers of genes as the median numbers of genes are equal in the 4 out of 5 cell types.  
 789 A similar pattern is observed on the Hi-C edge density. Specifically, the density is only significantly  
 790 different in two cell types: GM12878 and NHEK ( $p \leq 0.04$ ), although the difference is small (the median  
 791 density is 0.015 in GM12878 and 0.028 in NHEK) (Fig. S11B). However, the identified HIMs by the two  
 792 motifs are very different in other features. Compared to the HIMs identified by the triangle motif, the  
 793 HIMs identified by the 4-node motif  $M$  have much higher numbers of TFs ( $p \leq 2.45e-21$ ). The differ-  
 794 ence in the median number of TFs ranges from 4 to 8 (Fig. S12). Even though the HIMs by the 4-node  
 795 motif  $M$  have higher number TFs, they have comparable numbers of genes as compared to the HIMs  
 796 from the triangle. They also have much higher triangle density and much higher 4-node motif  $M$  density  
 797 ( $p \leq 2.68e-02$  and  $p \leq 1.43e-03$ , respectively; Fig. S11B). The HIMs from  $M$  also have a higher proportion  
 798 of genes in the A compartment in 4 cell types ( $p \leq 2.18e-02$ ), are much earlier replicated ( $p \leq 6.74e-03$ ),  
 799 and have smaller replication timing coefficient of variation ( $p \leq 4.38e-05$ ) (Fig. S12).

800 Next, we compared the features after adjusting the number of TFs and the number of genes of the  
 801 identified HIMs. The HIMs by the 4-node motif have much higher numbers of TFs than the HIMs by the  
 802 triangle motif. The number of genes is slightly different in some cell types. Since the features could be  
 803 biased to the number of TFs and the number of genes, we compared the features by adjusting the number  
 804 of genes and the number of TFs in HIMs by a linear regression model:

$$Y = \beta_0 + \beta_1 \times \# \text{TFs} + \beta_2 \times \# \text{genes} + \beta_3 \times \mathbb{1}_{\text{motif}}, \quad (11)$$

805 where  $Y$  is a given feature,  $\mathbb{1}_{\text{motif}} = 1$  if the HIM is identified with the 4-node motif  $M$ ,  $\mathbb{1}_{\text{motif}} = 0$  if  
 806 the HIM is identified with the triangle motif, and  $\hat{\beta}_3$  indicates the averaged difference in the feature  $Y$   
 807 between the HIMs identified by the two motifs after adjusting the number of TFs and the number of  
 808 genes in the HIMs. Specifically, a positive  $\hat{\beta}_3$  means that HIMs with the 4-node motif is higher in the  
 809 feature  $Y$  than the HIMs with the triangle motif. On the other hand, a negative  $\hat{\beta}_3$  means lower  $Y$  in  
 810 HIMs with the 4-node motif  $M$ . The detailed  $\hat{\beta}_3$  for the features are reported in the Table S4. Overall,  
 811 the differences are still significant after adjusting the number of TFs and the number of genes. Take  
 812 together, the 4-node motif  $M$  is better than the triangle motif in identifying HIMs.

### 813 B.3 HIMs share similar connections with 3D genome features across cell types

814 We found that the HIMs in 5 cell types in this study share similar connections with 3D genome organi-  
 815 zation features, such as A/B compartments, TADs, and loops. We looked at the genomic regions of each  
 816 HIM that is the smallest genomic block containing the transcription start sites of the genes in the HIM.  
 817 The median size of the genomic regions of the HIMs ranges from 4.9Mb in NHEK to 8Mb in GM12878  
 818 (Table S2), comparable to the size of A/B compartments (median size is 5Mb). The median numbers  
 819 of TADs in the genomic regions of the HIMs are 3-4 in different cell types (Table S2). The genomic  
 820 regions of the HIMs have, on average, 7 chromatin loops in GM12878 and 2-4 loops in the other cell  
 821 types (Table S2). The HIMs in GM12878 involve a higher number of loops, which perhaps is due to the

822 fact that GM12878 has at least 60% more detected loops than the other cell types possibly due to higher  
823 sequencing depth [6].

**Table S1:** Summary of the input heterogeneous networks and the identified HIMs across five cell types. ‘Overlapping HIMs (%)’ is the proportion of identified HIMs that share TFs with other HIMs. ‘Genes in HIMs (%)’ represents the proportion of genes in a heterogeneous network that are assigned to HIMs.

		GM12878	HeLa	HUVEC	K562	NHEK
Input	TFs	591	591	591	591	591
	Genes	11,627	12,036	11,927	12,391	12,161
	TF→gene	1,078,893	998,174	828,303	1,119,395	814,017
	Gene–gene	337,036	164,007	184,866	253,218	139,385
Output	HIMs	650	806	773	802	664
	Overlapping HIMs (%)	72.8	74.7	71.9	74.7	79.4
	Genes in HIMs (%)	69.1	77.2	75.3	76.5	62.1

**Table S2:** Statistics of the identified HIMs across five cell types.

	GM12878	HeLa	HUVEC	K562	NHEK
Median TF number	9	17	17	15	14
Median gene number	9	9	9	9	9
Median loop number	7	2	2	4	2
Median TAD number	4	3	3	4	3
Median 1D distance between The farthest apart genes (Mb)	8	5.4	6.1	7.2	4.9
# of HIMs inherited TFs	451	599	546	596	497
Median proportion of inherited TFs	28.6	27.8	24.6	25.0	28.0

**Table S3:** The dynamics of chromatin interaction networks and GRNs across 5 cell types. Cells in the table are numbers/proportions of interactions that exist in the corresponding number of cell type in each column. For example, column ‘1’ corresponds to the interactions that only exist in one cell type. Column ‘5’ corresponds to the interactions that exist in all 5 different cell types. Overall, a large proportion of the edges in the GRNs and chromatin interaction networks only exist in one cell type.

	Type	1	2	3	4	5
Hi-C networks	# interactions	755,574	242,833	86,790	36,945	23,442
	% of interactions	66.00	21.20	7.60	3.20	2.00
GRNs	# interactions	637,950	457,289	309,733	234,033	389,722
	% of interactions	31.40	22.50	15.30	11.50	19.20

**Table S4:** Comparison between the identified HIMs by the 4-node motif  $M$  and the triangle motif while adjusting the numbers of TFs and genes in the HIMs by the linear regression model  $Y = \beta_0 + \beta_1 \times \# \text{TFs} + \beta_2 \times \# \text{genes} + \beta_3 \times \mathbb{1}_{\text{motif}}$ , where  $Y$  is a continuous feature,  $\mathbb{1}_{\text{motif}} = 1$  if a HIM is identified by the 4-node motif  $M$  and 0 otherwise,  $\hat{\beta}_3 \geq 0$  means that the HIMs identified by the 4-node motif  $M$  have higher  $Y$  than the HIMs identified by the triangle motif after adjusting the numbers of TFs and genes. P-value is computed for the hypothesis that  $\beta_3 \neq 0$ . The features with P-value  $< 0.05$  across 5 cell types are highlighted with bold font.

Y	GM12878		HeLa		HUVEC		K562		NHEK	
	$\beta_3$	P value								
Hi-C edge density	0.005	5.86e-01	0.012	1.55e-01	0.02	1.51e-02	-0.001	9.03e-01	0.026	3.02e-03
<b>Triangle density</b>	0.11	9.9e-17	0.071	3.19e-10	0.074	6.04e-11	0.056	4.45e-07	0.077	1.43e-11
<b>4-node motif <math>M</math> density</b>	0.15	1.93e-22	0.082	1.83e-11	0.089	6.25e-13	0.074	1.35e-09	0.09	6.91e-13
% of genes in A compartment	0.038	3.61e-04	0.036	8.4e-03	0.022	1.47e-01	0.033	7.81e-04	0.015	2.89e-01
<b>Mean replication timing</b>	2.76	8.87e-07	2.269	1.36e-08	2.485	2.59e-06	2.527	2.13e-07	2.673	1e-10
<b>Replication timing CV</b>	-0.04	3.27e-13	-0.029	6.88e-09	-0.032	8.82e-10	-0.029	2.03e-09	-0.029	9.36e-12

**Table S5:** The top GO terms or pathways that are enriched in the genes that are assigned to HIMs consistently or in a cell type-specific manner. The number of genes in each category is shown in Fig. 4A.

	GO term/Pathway	Count	Fold Enrichment	P value
<b>Constitutive genes</b>	chromosome organization	371	1.50	5.7e-19
	macromolecular complex subunit organization	653	1.30	1.2e-12
	regulation of gene expression, epigenetic	105	1.90	3.4e-12
	RNA processing	287	1.40	4.1e-12
	nucleosome organization	74	2.10	4.2e-12
	DNA conformation change	104	1.80	2.2e-11
	mRNA processing	163	1.60	9.3e-11
	protein-DNA complex subunit organization	98	1.80	2.0e-10
	DNA packaging	77	1.90	5.2e-10
	mRNA metabolic process	213	1.40	2.5e-9
	RNA splicing	139	1.60	3.4e-9
	protein localization to organelle	268	1.40	4.2e-9
<b>GM12878 specific genes</b>	intracellular transport	436	1.30	6.5e-9
	regulation of lymphocyte activation	28	3.40	6.5e-8
	regulation of T cell activation	24	3.80	7.4e-8
	regulation of leukocyte cell-cell adhesion	24	3.60	1.8e-7
<b>HeLa specific genes</b>	T cell activation	28	3.00	5.5e-7
	cell development	74	1.50	4.8e-4
<b>K562 specific genes</b>	cell-cell signaling	57	1.60	5.6e-4
	phospholipase C-activating G-protein coupled receptor signaling pathway	11	4.80	8.5e-5
	reproduction	55	1.70	1.3e-4
	G-protein coupled receptor signaling pathway	33	2.00	1.7e-4
<b>NHEK specific genes</b>	keratinocyte differentiation	23	10.30	2.5e-16
	skin development	30	6.60	1.2e-15
	keratinization	16	18.30	2.0e-15
	peptide cross-linking	16	17.00	7.0e-15
	epidermis development	32	5.60	2.6e-14

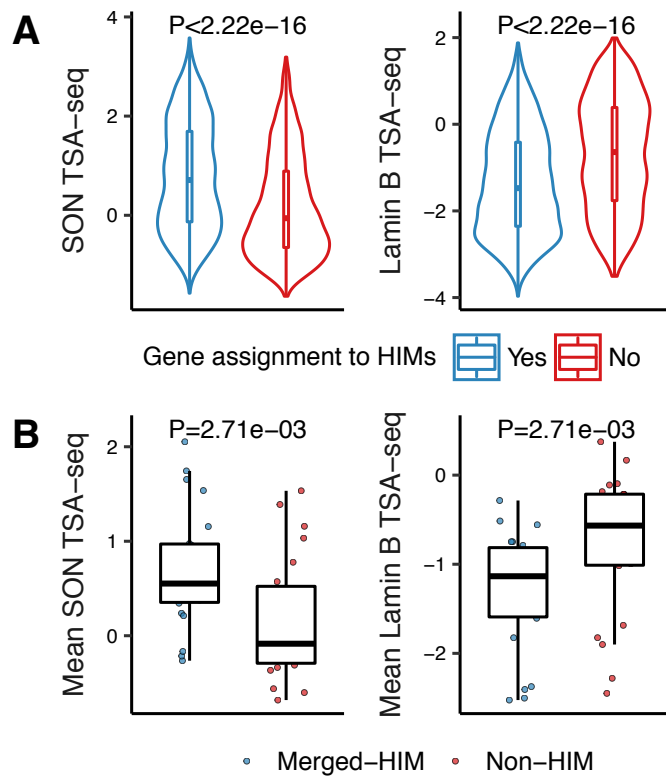


**Figure S1:** Genes assigned to HIMs are closer to nuclear speckles as compared to the genes in the heterogeneous network that are not assigned to HIMs in K562. **(A)** Violin plots show the distributions of TSA-seq scores of the two sets of genes. **(B)** Boxplots show the distributions of mean TSA-seq scores of the merged-HIM clusters and non-HIM clusters. Here we merged the genes assigned to HIMs on the same chromosome into one cluster and called it a merged-HIM cluster. Similarly, we merged the genes not assigned to HIMs on the same chromosome into one cluster and called it a non-HIM cluster.

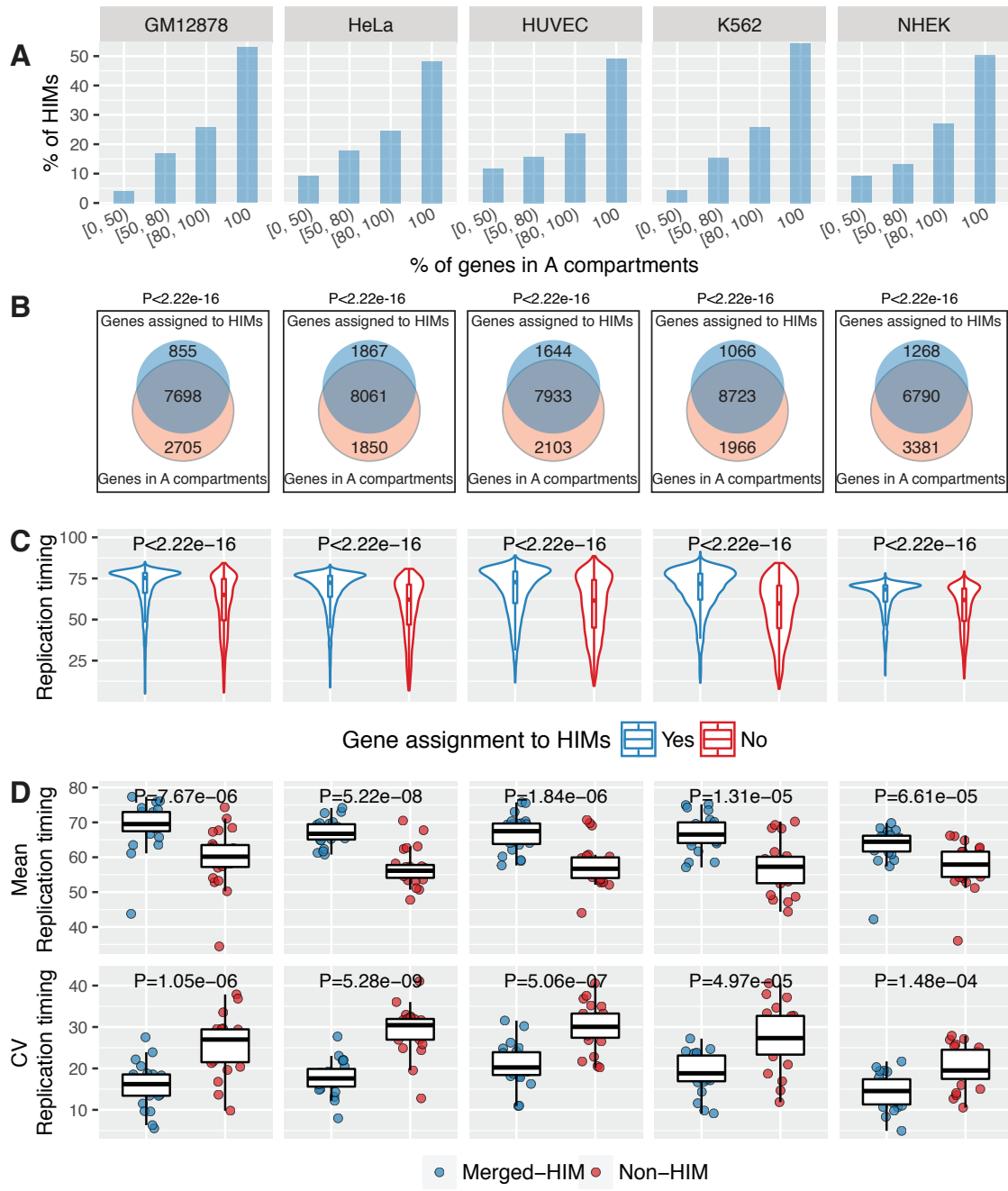


**Figure S2:** HIMs consistently have spatial location preferences as compared to non-HIMs in five cell types. Rows correspond to the spatial location features. Columns correspond to the cell types. **(A)** Barplot shows the distribution of HIMs with a varied proportion of genes that are in A compartment. **(B)** Venn diagram shows that the genes assigned to HIMs, as a whole, are enriched with the genes in A compartment. **(C)** Boxplots compare the replication timing of the genes that are assigned to HIMs against the genes that are not assigned to HIMs. **(D)** Boxplots show the mean and coefficient of variation (CV) of replication timing of the genes in merged-HIMs or non-HIMs. Each dot represents a merged-HIM or non-HIM. A lower CV means that the genes in a cluster have a lower variability in replication timing thus they are more likely to be replicated synchronously.

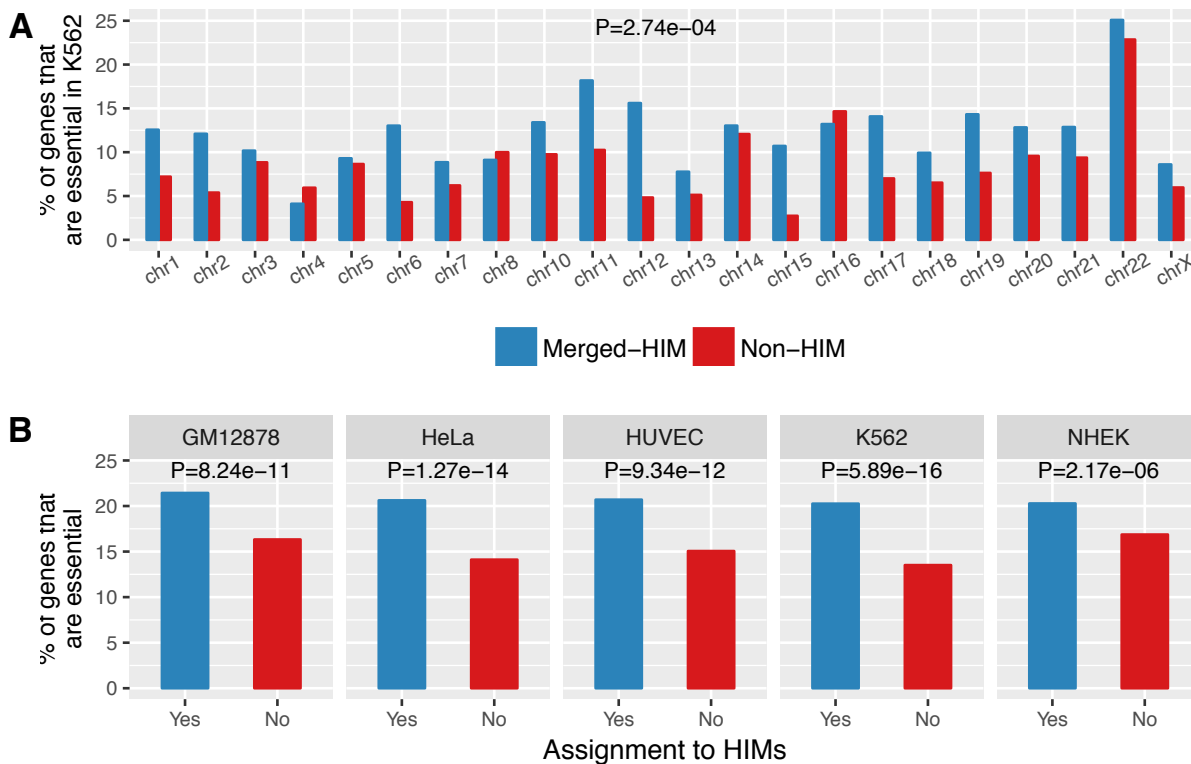


**Figure S3:** HIMs have more essential genes across cell types. **(A)** Barplots show the proportions of genes that are K562 essential genes in the genes assigned to HIMs and the genes not assigned to HIMs. **(B)** Barplots show the proportions of K562 essential genes in merged-HIMs and non-HIMs across the chromosomes. The P-value is computed by the paired two-sample Wilcoxon rank-sum test. **(C)** Barplots show the proportions of essential genes in the genes assigned to HIMs and the genes not assigned to HIMs. P-value is computed by the Chi-squared test of independence. The proportions of the essential genes in merged-HIMs and non-HIMs are similar to **(A)** thus are not shown here.

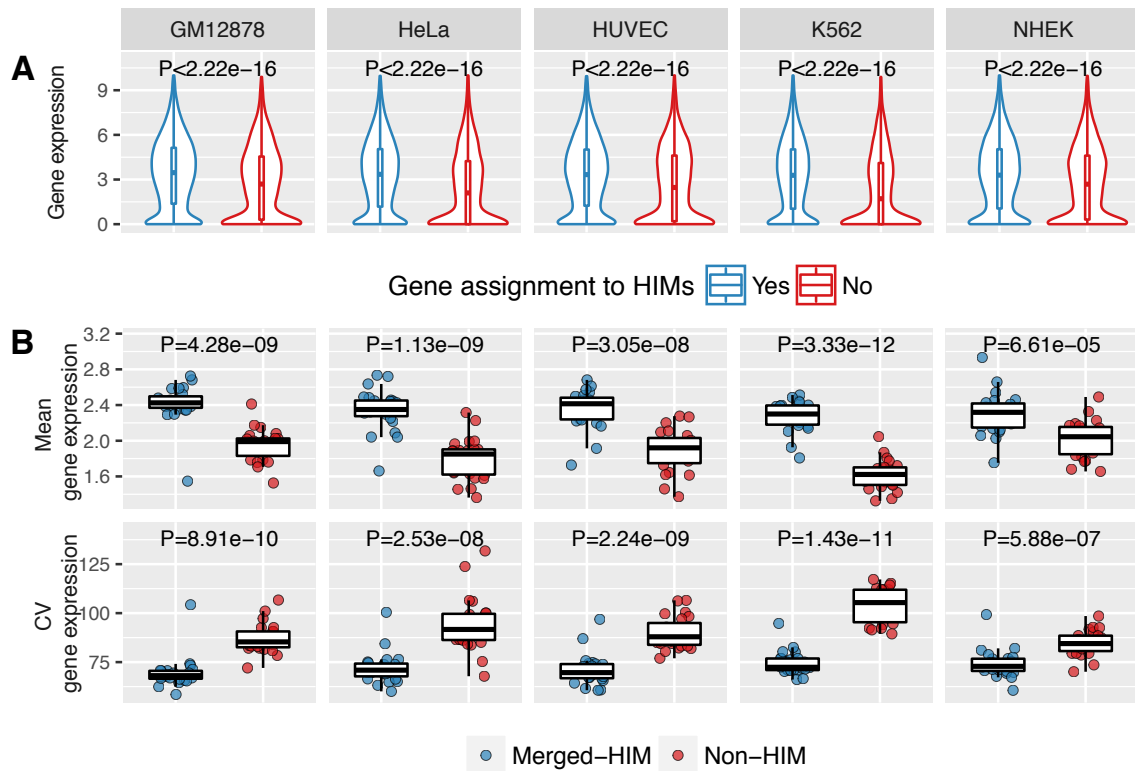


**Figure S4:** The genes assigned to HIMs express at higher levels than the genes not assigned to HIMs across cell types. **(A)** Violin plots show that the genes assigned to HIMs, as a whole, are more expressed than the genes not assigned to HIMs. **(B)** Boxplots show that the merged-HIMs have higher mean and lower CV of expression level than the non-HIMs.

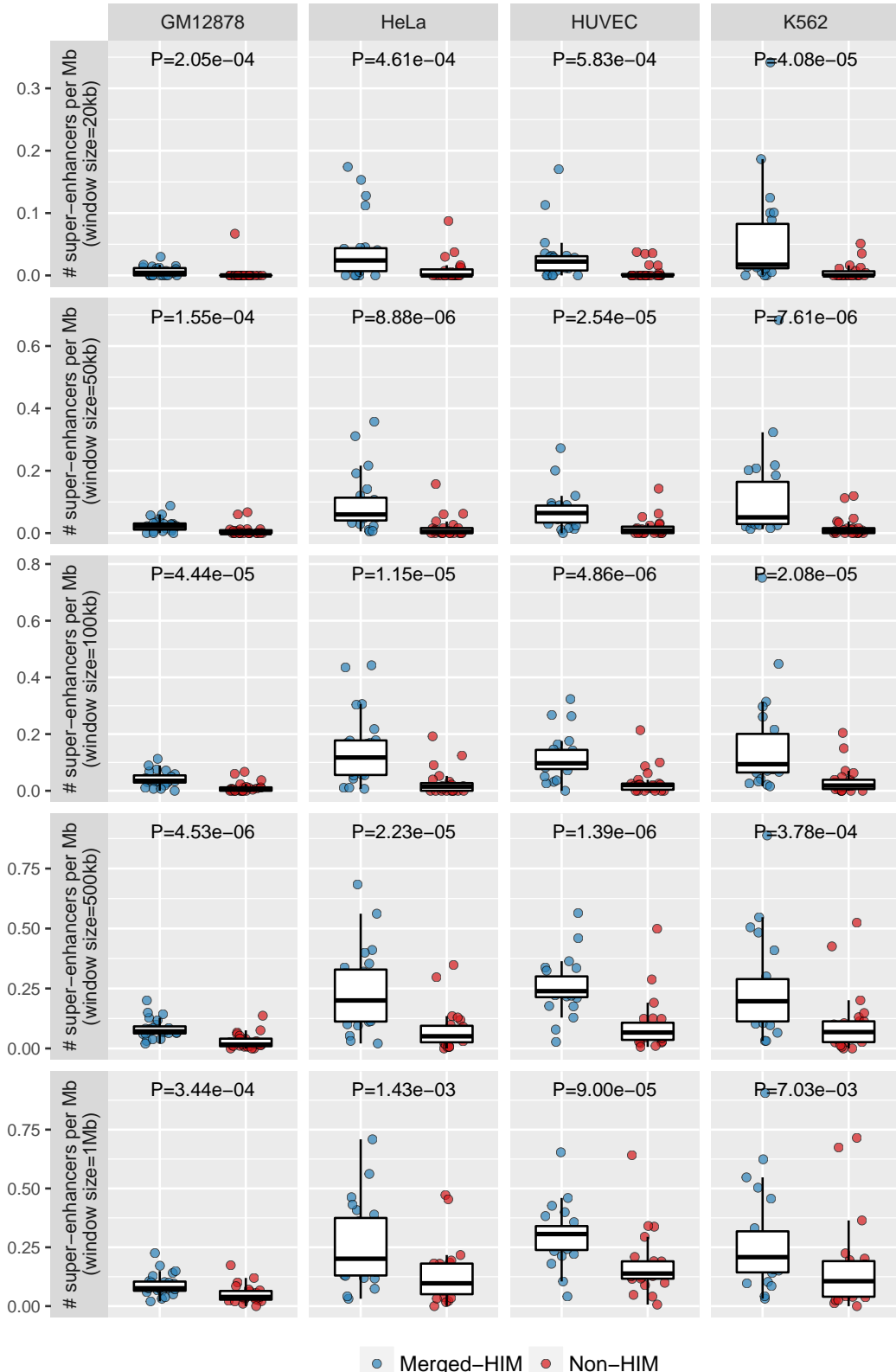


**Figure S5:** HIMs are enriched with super-enhancers and this observation is robust to the window size. The window size is used to define the genes that are close to a given super-enhancer. The window size ranges from 20kb to 1Mb. The distribution of super-enhancers in NHEK is missing due to lack of super-enhancer data in NHEK.

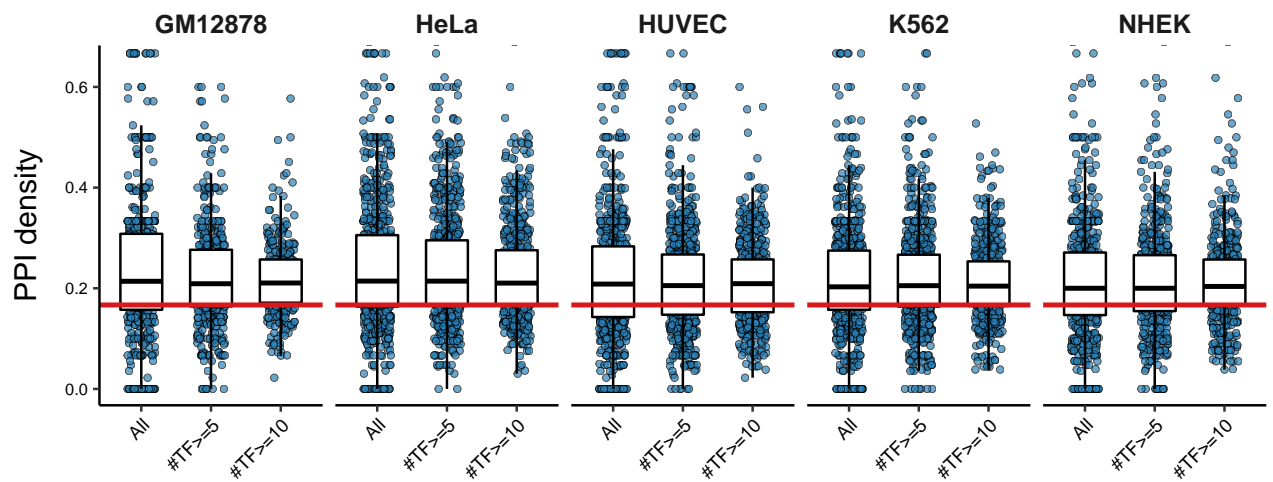


**Figure S6:** TFs in HIMs are enriched with protein-protein interactions (PPIs). Boxplots show the distribution of the sub-PPI network density across HIMs and subsets of HIMs with at least  $n$  TFs,  $n = 5, 10$ . Here for each HIM, we computed the density of the sub-PPI network induced by the TFs in the HIM from the PPI network based on 591 TF proteins used in this study. The medians are all higher than the expected density (0.158, red line) of the sub-PPI networks induced by randomly sampled TFs ( $p < 2.22e-16$ ).

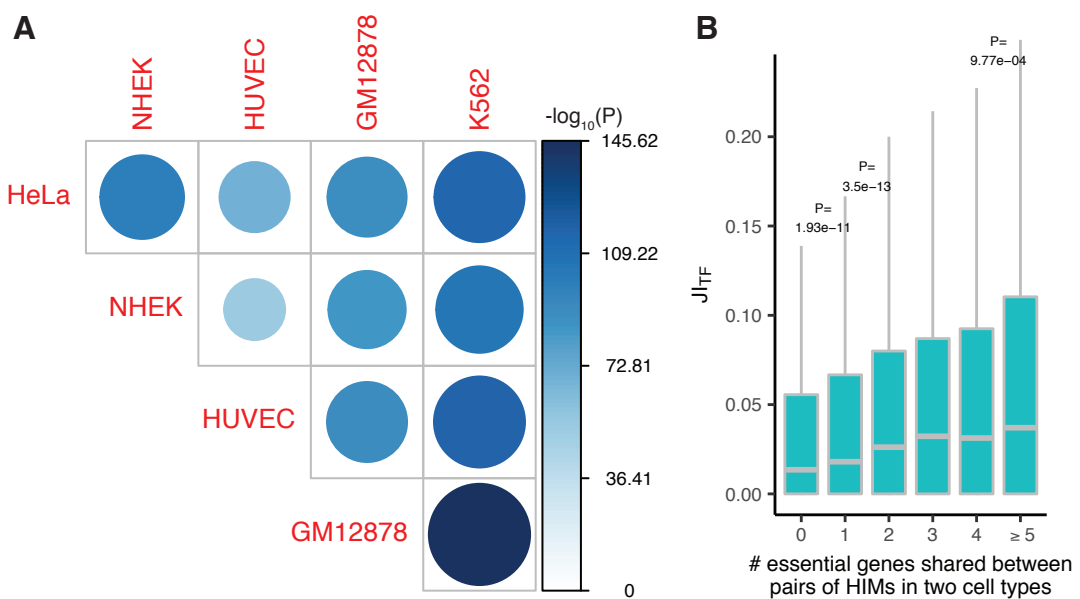


**Figure S7:** HIM comparisons regarding genes and TFs across cell types. **(A)** Heatmap shows the level of significance in overlapping between the genes assigned to HIMs in two different cell types. GM12878 and K562 have the highest overlap. Statistical significance is evaluated by the hypergeometric test. **(B)** Boxplots show the distribution of Jaccard index on the TFs of paired HIMs with different numbers of shared essential genes.

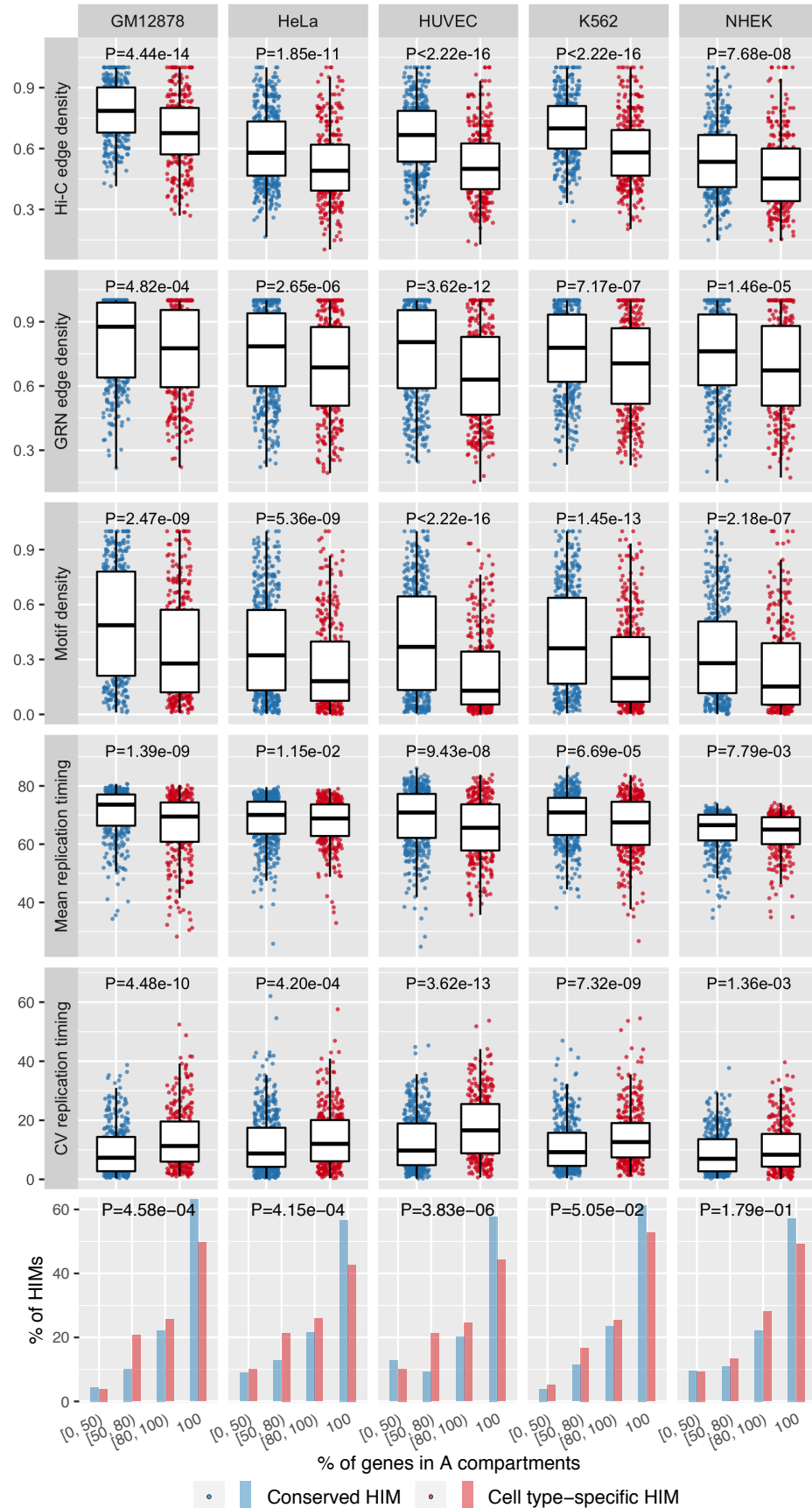


**Figure S8:** Conserved and cell type-specific HIMs have distinct spatial location features.

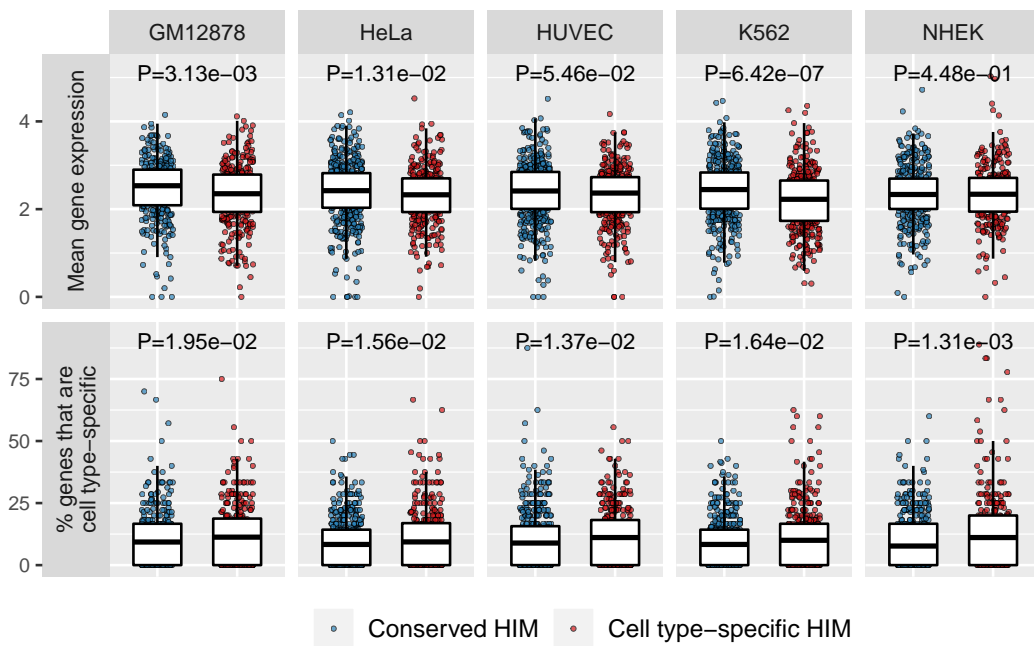


**Figure S9:** Functional differences and similarities between conserved and cell type-specific HIMs. Conserved HIMs have higher average gene expression in 3 cell types (first row). On the other hand, cell type-specific HIMs tend to have a higher proportion of cell type-specific genes in all 5 cell types (second row).

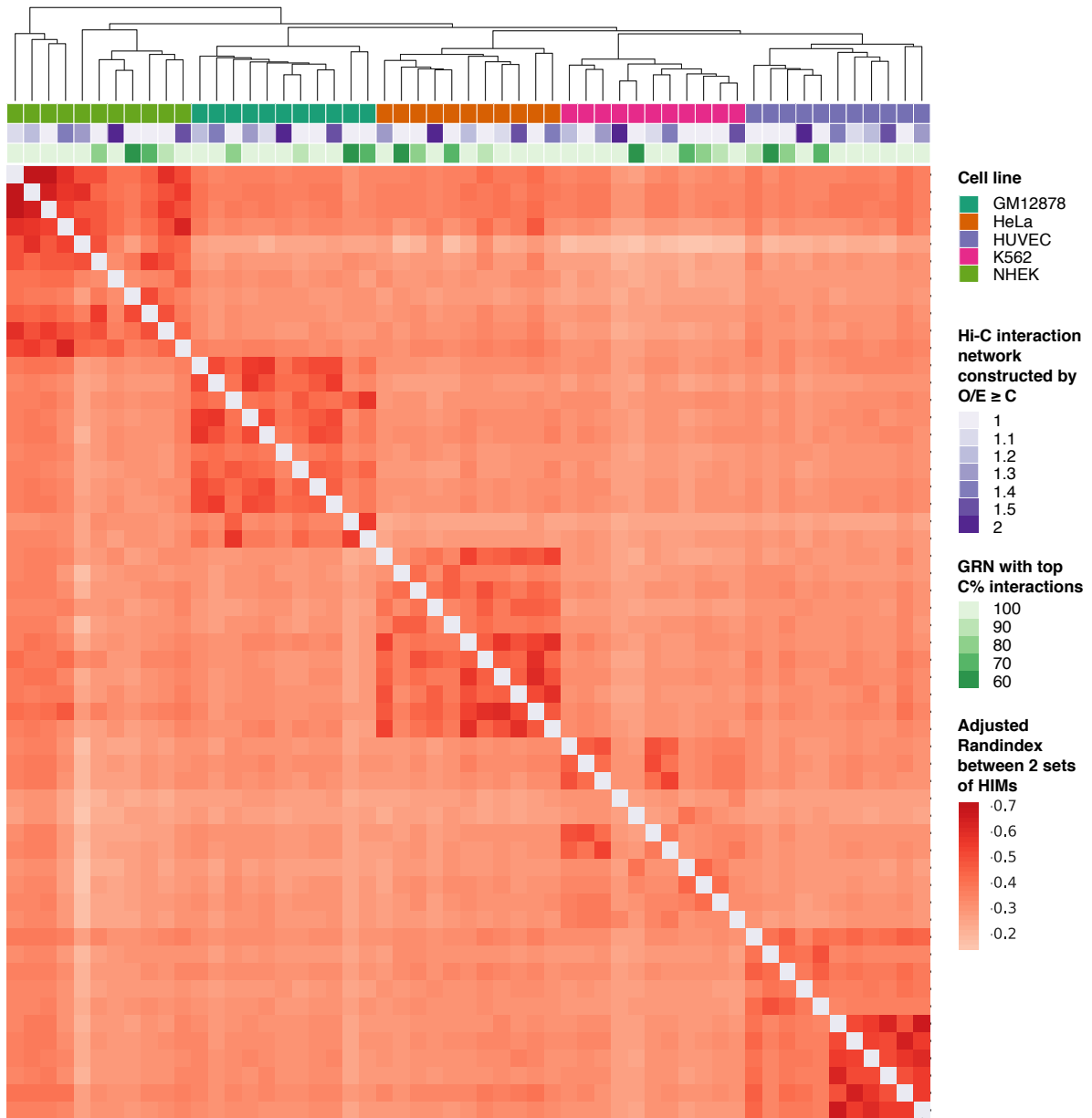


**Figure S10:** HIMs are robust to the input heterogeneous networks. For each cell type, there are 3 heterogeneous networks: one used in the main text and two sub-heterogeneous networks derived from different combinations of Hi-C interaction networks and GRNs. A sub-Hi-C represents a sub-Hi-C interaction network with interactions satisfying  $O/E \geq 2$ . The sub-GRN represents a sub-GRN with interactions having top 90% scores. The heterogeneous network (Hi-C + GRN) is used in the main text. The other two (sub-Hi-C + GRN, Hi-C + sub-GRN) are sub-heterogeneous networks. Adjusted Rand index is used to quantify similarities on gene memberships between two different sets of HIMs that are resulted from two different heterogeneous networks. Then hierarchical clustering on adjusted Rand index is used to cluster the sets of HIMs. Overall, the result shows that the sets of HIMs from the same cell type are in the same cluster thus are much more similar as compared to the sets of HIMs from different cell types.

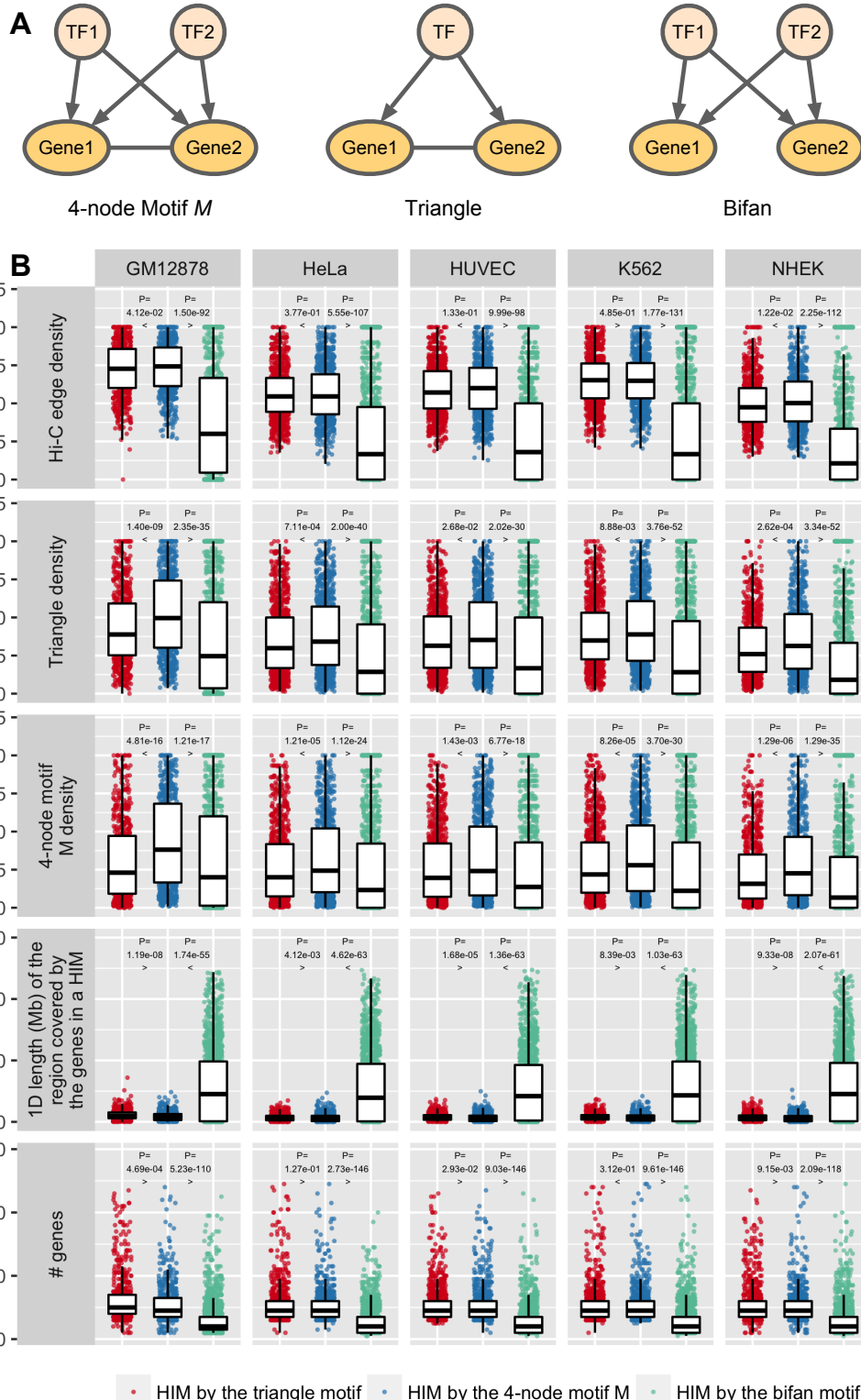


**Figure S11:** Comparison of the identified HIMs between the 4-node motif  $M$ , a triangle motif, bifan motif across 5 cell types. **(A)** Illustration of the 3 different motifs. **(B)** Comparison between the HIMs identified by the 3 different motifs. Rows correspond to the features. Columns correspond to the cell types. Each dot represents a HIM.

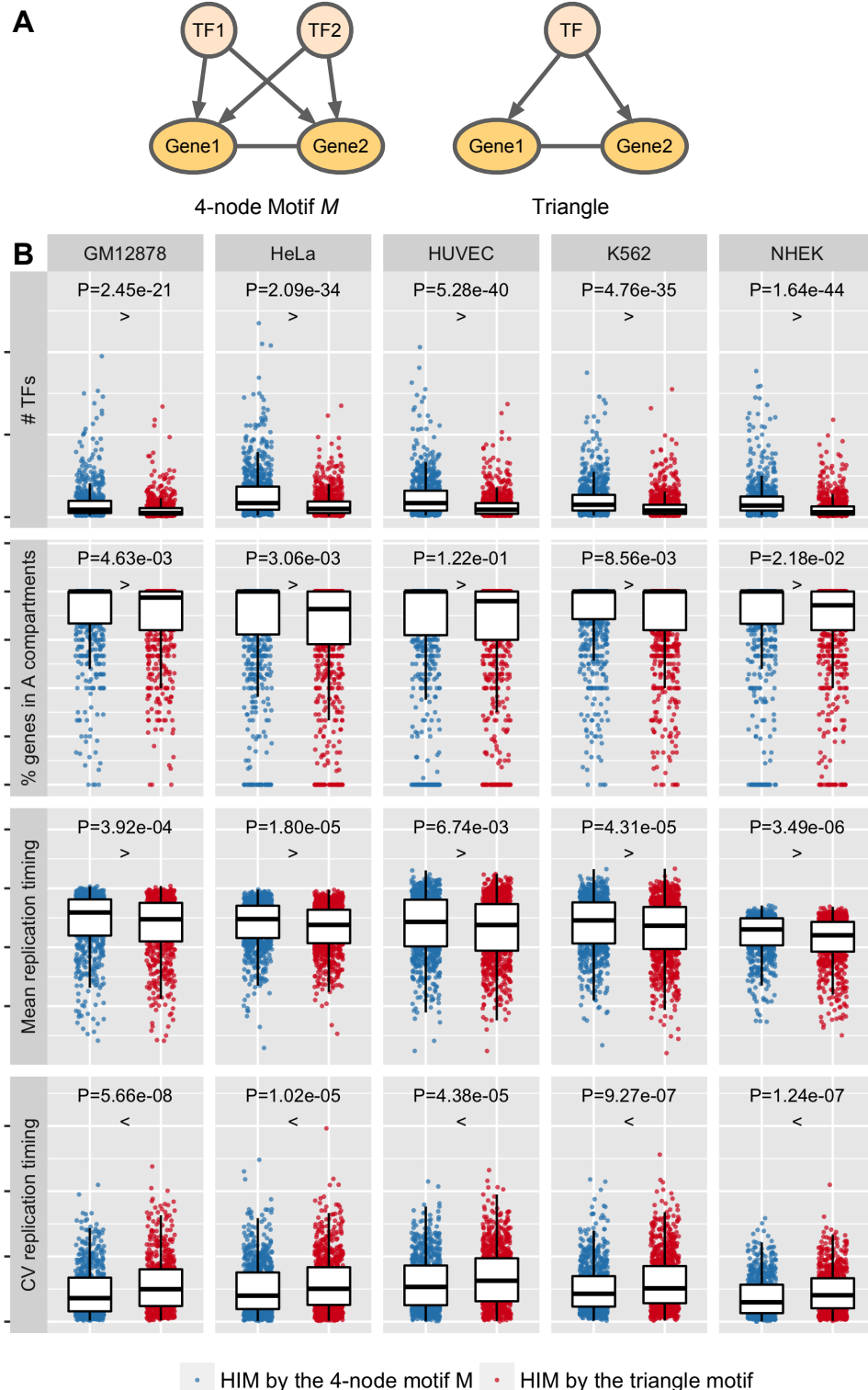


**Figure S12:** Comparison of identified HIMs between the 4-node motif  $M$  and the triangle motif across the 5 cell types. Where the triangle motif has 3 nodes (**A**). Two of them are genes connected by a chromatin interaction and co-regulated by a TF. (**B**) Rows correspond to the features. Columns correspond to the cell types. Each dot represents a HIM identified either by the 4-node motif  $M$  or the triangle motif. The patterns are consistently observed after adjusting the numbers of TFs and genes in HIMs by a linear regression model (Table S4).